Drug Design, Development and Therapy

Dovepress
Taylor & Francis Group

Open Access Full Text Article

ORIGINAL RESEARCH

Mechanistic Insights into FOLFOX-Induced Neurotoxicity and Determination of Its Concentrations via a Novel, Simultaneous HPLC Quantification Method in Brain Tissue

Rasha A Mansouri[1,2], Adel M Ahmed[3], Huda F Alshaibi[2,4], Wafaa M Fouda[5], Esam M Aboubakr[6]

[1]Chemistry Department, Faculty of Science and Humanities, Prince Sattam bin Abdulaziz University, Al-Kharj, Saudi Arabia; [2]Biochemistry Department, Faculty of Sciences, King Abdulaziz University, Jeddah, Saudi Arabia; [3]Department of Pharmaceutical Analytical Chemistry, Faculty of Pharmacy, South Valley University, Qena, Egypt; [4]Embryonic Stem Cell Unit, King Fahd Medical Research Center, King Abdulaziz University, Jeddah, Saudi Arabia; [5]Department of Pharmacology and Toxicology, Faculty of Pharmacy, University of Sadat City, Sadat, Egypt; [6]Department of Pharmacology and Toxicology, Faculty of Pharmacy, South Valley University, Qena, Egypt

Correspondence: Esam M Aboubakr, Email esam_pharma@svu.edu.eg

Background: FOLFOX, a commonly prescribed chemotherapeutic regimen, associated with significant neurotoxicity, that necessitates stop administration in some cases, hence, this study aimed to investigate the molecular mechanisms underlying FOLFOX-induced neurotoxicity in the brain and sciatic nerve, and determining its cerebral concentration via HPLC technique.

Methods: 48 rats were divided into four groups: normal control, Oxaliplatin (6 mg/kg), 5-Fluorouracil (50 mg/kg), and a combination group (oxaliplatin 6 mg/kg + 5-fluorouracil 50 mg/kg). Behavioral tests in addition to samples collection from cerebral tissues, sciatic nerves, and blood were conducted. Tissue histological and biochemical changes were determined, including oxidative stress markers (Nrf2, SOD2, HO-1), apoptotic proteins (Bax, cCaspase-3, Bcl-2), and inflammatory biomarkers (COX-II, TNF-α, IL-6, NF-κβ). A new HPLC method was developed and validated to quantify oxaliplatin and 5-fluorouracil (5-Flu) concentrations in the brain tissue.

Results: Both oxaliplatin and 5-Flu induced a substantial oxidative stress, evidenced by reduced expression of Nrf2, SOD2, and HO-1 proteins, associated with a significant upregulation of the pro-apoptotic proteins Bax and cleaved caspase-3, and downregulation of the anti-apoptotic protein Bcl-2. Inflammatory markers were increased in all treated groups, and the highest levels were observed in the combination group. HPLC analysis confirmed a significantly higher concentration of both drugs in the cerebral tissue of the combination group. Histopathological findings revealed neuronal damage and inflammation associated by increased Glial fibrillary acidic protein (GFAP) and decreased neural cell adhesion molecule (NCAM) expression. Behavioral assessments demonstrated markedly reduced pain thresholds in treated animals.

Conclusion: This study identified a novel mechanisms underlying FOLFOX neurotoxicity involving activation of the pro-apoptotic BAX/cCaspase-3 pathway and suppression of the Nrf2/KEAP-1/SOD2/HO-1 antioxidant defense mechanism. These disorders induced a neuronal injury, evidenced by altered GFAP and NCAM expression. The findings highlight the synergistic role of FOLFOX components in driving oxidative stress, apoptosis, and inflammation, collectively contributing to neurotoxicity.

Keywords: FOLFOX, oxaliplatin, 5-fluorouracil, neuronal damage, HPLC, GFAP, NCAM

Introduction

An increased number of a new cancer patients are diagnosed every year, millions of cancer-related deaths occur annually, and the global cancer burden is expected to continue rising in the following years.[1] The use of chemotherapy as a primary treatment or as a component of combination therapy is a major approach in the treatment of cancer. Unfortunately, chemotherapy administration can also induce unexpected adverse events, resulting in chemotherapy-induced neuronal tissue toxicity,[2] that can present in several forms, including headache, severe pain, vision loss, seizures, cerebellar dysfunction, and spinal cord injury accompanied by myelopathy.[3] The neurotoxicity of a wide range of commonly used

Received: 10 May 2025
Accepted: 29 September 2025
Published: 6 October 2025

chemotherapeutic drugs, such as platinum compounds, anthracyclines, vinca alkaloids, and thalidomide, has been documented to vary and can induce sever neurological disorders with prolonged use.[4,5]

FOLFOX, a combination of folinic acid, fluorouracil (5-Flu), and oxaliplatin,[6] is commonly administered in different types of cancer, It has been reported to induce significant side effects, that can lead to the discontinuation of the regimen.[6] Oxaliplatin is a platinum-based compound that disrupts DNA synthesis mainly by inducing intrastrand cross-links within genomic DNA, exhibiting a wide range of antineoplastic effects. Clinically, oxaliplatin is used in several chemotherapy regimens, mostly for the treatment of pancreatic, gastric, and colorectal cancer, with significant efficacy.[7]

5-Flu is an antimetabolite drug widely used to treat cancer, particularly colorectal cancer. 5-Flu is a heterocyclic aromatic organic molecule similar to uracil. Its pyrimidine-like structure makes it an antimetabolite that can be readily integrated into DNA and RNA as a substitute for thymine or uracil.[8] Thus, it induces cell cycle arrest, specifically in the S phase, suppresses the ability of cancer cells to multiply, and triggers apoptosis.[9]

Apoptotic cell death is a fundamental physiological process that selectively eliminates cells.[10] Caspase-3 is a crucial agent in cell apoptosis, serving as the primary initiator and executor of apoptosis. It is considered the essential pathway for the sequential action of apoptotic proteases,[11] and is the pivotal protease positioned downstream in the caspase cascade process responsible for initiating apoptosis. However, the proteins Bcl-2 and Bax, belonging to the Bcl-2 family, have the ability to impede the activation of caspase and perform significant functions in preventing apoptosis and oxidation.[12]

Oxidative stress can potentially disturb the function and survival of neuronal and non-neuronal cells in the nervous system by altering proteins, lipids, and nucleic acids.[13,14] Nuclear factor-erythroid-2-related factor 2 (Nrf2) is a transcription factor that controls the expression of several genes linked to antioxidants and cytoprotection.[15,16] Under normal circumstances, Nrf2 is localized in the cytoplasm through its interaction with the inhibitor Kelch-like ECH-associated protein 1 (Keap-1). The regulation of Nrf2 expression is accomplished by the processes of Keap-1-mediated ubiquitylation and proteasomal degradation. Nuclear translocation of released Nrf2 triggers the transcription of genes encoding anti-oxidative and detoxifying enzymes such as superoxide dismutase (SOD).[17,18] Enhanced expression of these detoxifying and antioxidant proteins amplifies the cellular capacity to counteract reactive oxygen species (ROS).[19]

High-performance liquid chromatography (HPLC) is a prevalent analytical technique used for quantifying drugs in brain tissue, owing to its exceptional sensitivity, selectivity, and reliability.[20] Using HPLC permit to precisely quantify the levels of dugs and their metabolites in intricate biological matrices, such as brain homogenates, which is essential for pharmacokinetic and neuropharmacological studies such as detection of Ochratoxin A (a neurotoxin) in mouse brain for neurodegeneration research,[21] determination of antiepileptics (*eg*, valproic acid) in mouse brain homogenates,[22] and the measurement of neurotransmitter metabolites such as 3-Methoxytyramine (3-MT) in rat brain homogenates with an isocratic HPLC method.[23] The highly sensitivity and reproducibility of HPLC results render it invaluable for investigating blood-brain barrier permeability, drug distribution, and clearance from cerebral tissue.[23,24] The methodology facilitates method validation for selectivity, linearity, accuracy, precision, and stability, thereby ensuring dependable results for drug quantification in preclinical and clinical research environments.[24,25]

Previous HPLC-based attempts to quantify drugs in brain tissue have been limited. For oxaliplatin, reversed-phase HPLC with UV detection was applied to plasma (linear range: 0.3–125 μg/mL) after protein precipitation, but the method was neither validated for brain tissue nor for concentrations below 0.3 μg/mL.[26] Similarly, while 5-FU has been measured in plasma using UHPLC–MS/MS with low detection limits (0.1–0.2 μg/mL), these approaches rely on protein removal and matrix-matched calibration in plasma or cell cultures, leaving lipid-rich brain matrix effects unaddressed.[27] Critically, no HPLC or LC-MS method has simultaneously quantified intact oxaliplatin and 5-FU in any biological matrix, underscoring the unmet need for brain-specific assays.

Despite FOLFOX's known neurotoxic potential, the specific oxidative and apoptotic pathways involved remain poorly defined in vivo, hence the present study combines HPLC with mechanistic analyses to uncover biomarkers and molecular pathways linked to FOLFOX-associated neurotoxicity. These insights may guide therapeutic strategies to reduce adverse effects during chemotherapy. The newly optimized HPLC protocol achieved first-time simultaneous

quantification of both drugs in neuronal tissue homogenates, enabling detailed analysis of their tissue distribution, and relationship to neurotoxic outcomes.

Materials and Methods

Chemicals and Reagents

HPLC-grade solvents (propanol, butanol, methanol, acetonitrile) and analytical-grade reagents (sodium acetate, disodium hydrogen phosphate) were purchased from Merck (Darmstadt, Germany). Ultrapure water was produced using a Milli-Q Plus® water purification system (Millipore, Milford, MA, USA). Stock solutions (10 mg/L) of oxaliplatin and 5-Flu were prepared by individually dissolving each drug in 10 mL of mobile phase. Working standards were then prepared by diluting the stock solutions with HPLC mobile phase as required.

HPLC Method

Chromatographic analysis was performed using an Agilent 1260 Infinity® HPLC system (Agilent Technologies, Germany), equipped with a binary solvent pump, thermo-stated column compartment, autosampler, and diode array detector. System control and data processing were managed via OpenLAB CDS ChemStation® software. Mobile phases and sample solutions were ultrasonically degassed (WUC-D03H, DAIHAN Scientific, Korea) and filtered through 0.45 μm nylon membranes (PALL Life Sciences, USA).

Oxaliplatin and 5-Flu were quantified under isocratic conditions at 30°C using a Pursuit-3® C18 column (150 mm × 4.6 mm id., 3 μm particle size; Agilent Technologies, Netherlands). The mobile phase comprised 3% (v/v) propanol and 97% (v/v) 0.1 M acetate buffer (pH 3.5) containing 0.08% SDS, delivered at a flow rate of 0.8 mL/min. Injections of 10 μL standard solutions were analyzed with UV detection at 260 nm.

Chromatographic parameters (eg, mobile phase composition, column temperature, detection wavelength) were systematically optimized and validated in accordance with ICH Q2 (R1) guidelines to ensure method robustness, specificity, and linearity.

Calibration of Oxaliplatin and 5-Flu in Brain Tissue Homogenates

To 0.5 mL aliquots of brain homogenate, working solutions of oxaliplatin (0.3–130 μg/mL) and 5-Flu (0.01–25 μg/mL) were added. The mixtures were vortex-mixed for 3 minutes and centrifuged at 6000 rpm for 5 minutes at room temperature. Following centrifugation, the mobile phase was added to achieve a final volume of 10 mL. The solution was thoroughly mixed and filtered through a 0.22 μm syringe filter. A 10 μL aliquot of the resulting clear supernatant was injected into the HPLC system for analysis.

Study Design

Forty-eight male Sprague-Dawley rats (140–150 g) were gained from the Egyptian Organization for Biological Products and Vaccines (Giza, Egypt) and housed under standard laboratory conditions. Rats were acclimatized for 10 days prior to experimentation, with ad libitum access to food and water. Animals were randomly assigned to treatment groups (n = 12). The experimental protocol was approved by the Ethical Committee of the Faculty of Pharmacy, South Valley University (Approval No. P.S.U.V 019/23) and conducted in compliance with the International Association for the Study of Pain guidelines for animal research.[28] To minimize bias, behavioral assessments were performed by independent researchers blinded to treatment assignments.

Experimental Groups

After the end of the acclimatization period, and following Animal Research: Reporting In Vivo Experiments (ARRIVE) human endpoints guidelines including; animals advanced lethargy, anorexia, dehydration, difficulty breathing rats, body weight reduction, Self-induced Trauma, Inability to Reach Food and Water, etc) animals were divided into the following groups:

1. Control group: animals were intraperitoneal (i.p) injected with 5% glucose followed by normal saline on a weekly basis for 6 weeks.
2. Oxaliplatin group: animals were i.p injected with 6 mg/kg of oxaliplatin dissolved in glucose on a weekly basis for 6 weeks.[29]
3. 5-Flu group: animals were i.p injected with 50 mg/kg 5-Flu dissolved in saline on a weekly basis for 6 weeks.[30]
4. Oxaliplatin + 5-Flu group: Rats were i.p injected with oxaliplatin (6 mg/kg) followed by 5-flu (50 mg/kg) 2 h later on a weekly basis for 6 weeks.[31]

Twenty-four hours after the final dose administration, animals were euthanized following ARRIVE and other international guidelines, adhering to ethical guidelines and animal welfare principles to ensure minimal animal suffering, using cervical dislocation under ether anesthesia. Blood was promptly collected via cardiac puncture and centrifuged at 3000 rpm for 10 minutes to isolate serum, which was stored at –80°C for subsequent biochemical analyses.

The brain was carefully dissected from the skull, and the right hemisphere was rinsed with ice-cold saline to remove residual blood. The tissue was then homogenized in 0.1 M phosphate buffer (pH 7.4) at a 1:10 (w/v) ratio. The homogenate was centrifuged at 3000 rpm, and the resulting supernatant was aliquoted and stored at –80°C for further analysis.

Histological Examination

Brain and sciatic nerve samples from each experimental group were fixed in 10% neutral-buffered formalin for 48 hours, followed by dehydration in graded concentrations of alcohol, cleared in xylene and subsequently processed for paraffin embedding, stored at 4 °C for subsequent analysis. Tissue sections were cut at 4–5 µm thickness by Microtome (Microm, Germany)., After deparaffinization and rehydration, hematoxylin solution was applied to the slides for 2 minutes and subsequently rinsed by running tap water for 5 minutes. Subsequently, the eosin solution was applied to the sections for 30 seconds, followed by thorough washing of the slides with running tap water, followed by dehydration. Six fields per section were randomly chosen and captured using the Olympus BX-61 microscope (Olympus, USA), by two independent pathologists. A minimum of four sections were chosen, spaced 100 µm apart, were selected (n = 6 rats per group) for the investigation. The following scoring analysis was followed: for fibrotic changes determination:[32,33] 1 = mild or nearly absent necrotic tissue, 2 = moderately observed necrotic tissue, 3= moderately severe necrotic tissue, and 4 = severe necrosis.[32,33]

For neuronal vacuolation, 1 = mild or nearly absent neuronal vacuolation, 2 = moderately observed neuronal vacuolation, 3= moderately neuronal vacuolation, and 4 = advanced neuronal vacuolation.[32,33]

For edema, 1 = mild or nearly absent edema, 2 = moderately observed edema, 3= moderately severe edema, and 4 = advanced edema.[32,33]

Assessments of Spontaneous Behaviors

To examine either oxaliplatin or 5-flu and how their combined administration (FOLFOX) can affect rats' behavior, the following tests were conducted on a bi-weekly basis; rats were acclimated for 30 min to the environment prior to each of the following test sessions.

Locomotor Activity (Locomotor)

Rats were placed individually into photocell activity cages (Columbus, OH) with dimensions of 28×16.5 cm. The interruption of photocell beams was recorded over 30 minutes, assessing the walking and rearing by rats.[34]

Paw Pressure Test

The assessment of mechano-hyperalgesia was conducted by utilizing a pressure stimulation approach with the aid of an analgesymeter (Ugo Basil, Milan, Italy) to measure the mechanical (static) nociceptive threshold. The rat's paw was subjected to mechanical pressure by placing it on a small plinth underneath the pusher with a rounded tip with cut-off pressure at 300 g. The operator recorded the force at which the rat experienced pain by releasing the pedal and reading the corresponding value from the scale.[35]

Allodynia Test

The tail-immersion test was used to measure thermal hyperalgesia and allodynia in cold water (4 −6 OC).[36] A 15-second cut-off time was used, and the length of tail-immersion in cold water before removal by rats was recorded.[37]

SOD Determination

The determination of superoxide dismutase (SOD) concentrations in the brain tissue involved the addition of 25 mL of supernatant produced from the centrifuged brain homogenate to a solution containing 1.2 mL of 0.052 M sodium pyrophosphate buffer (pH 8.3), 0.3 mL of 300 mM nitro blue tetrazolium, 0.1 mL of 186 mM phenazonium methiosulphate, and 0.2 mL of 780 mM NADH. The reaction mixtures were incubated for 2 min at a temperature of 32°C. The reaction was thereafter stopped by adding 0.1 mL of glacial acetic acid. The alterations in absorbance of the reaction mixture were assessed at a wavelength of 560 nm by spectrophotometer.[38]

Malondialdehyde (MDA) Determination

The quantification of MDA levels in brain tissue was performed depending on the determination of the color produced from the reaction between thiobarbituric acid (TBA) and MDA. To achieve this, a volume of 2.5 mL of a trichloroacetic acid solution (100 g/L) was introduced into a centrifuge tube containing 0.5 mL of the brain tissue supernatant. Subsequently, the tubes were immersed in a water bath set at boiling temperature for 15 min, followed by cooling using tap water. The tubes were centrifuged at 1000 rpm for 10 minutes. Subsequently, 2 mL of the resulting supernatant was added 1 mL of a TBA solution with a concentration of 6.7 g/L. The test tubes were then immersed in a water bath at boiling temperature for a period of 15 minutes. Subsequently, the solution underwent a cooling process in tap water, followed by the measurement of its absorbance using a spectrophotometer at a wavelength of 532 nm.[39]

Nitric Oxide Determination

The determination of nitric oxide content in the brain tissue relies on the utilization of Griess Reagents, which facilitate the conversion of nitrite into a highly azo compound exhibiting a deep purple color. The resulting azo dye was determined spectrophotometrically at 540 nm.[40]

Glutathione Peroxidase (GPx) Determination

Principally, cumene hydroperoxide is reduced by glutathione peroxidase (GPx), which oxidizes GSH to create GSSG. Glutathione reduces GSSG to generate GSH and uses NADPH in the process. GPx activity correlates directly with the decrease in NADPH (determined at 340 nm).[41]

Catalase Determination

Principally, the catalase enzyme reacts with a specific amount of hydrogen peroxide (H2O2); the reaction is terminated after one minute by adding a catalase inhibitor. In the presence of the enzyme peroxidase (HRP), remaining hydrogen peroxide (H2O2)f under-goes a reaction with 3,5-Dichloro-2-hydroxybenzene sulfonic acid (DHBS) and 4-aminophenazone (AAP) to produce a chromophore, the absorbance of the resulting dye was determined at 520 nm. The intensity of this chromophore's color is inversely related to the quantity of catalase present in the homogenate sample.[42]

Reduced Glutathione Determination

Reduced glutathione (GSH) concentrations in the brain homogenate were determined briefly as follows: samples were subjected to precipitation using a 50% solution of trichloroacetic acid, followed by centrifugation at a speed of 1000 rpm for 5 minutes. The reaction mixture consisted of 0.5 milliliters of supernatant, 2.0 milliliters of Tris-EDTA buffer (0.2 M, pH= 8.9), and 0.1 milliliters of a 0.01 M solution of 5,5′-dithiobis (2-nitrobenzoic acid). The solution was maintained at 28 OC for a duration of 5 minutes; the produced color was determined using spectrophotometric analysis at a wavelength of 412 nm.[43]

Enzyme-Linked Immunosorbent Assay (ELISA)

In the present study, ELISA technique was applied to determine the effect of FOLFOX administration and its induvial component on the following parameters using a standard kit; Tumor Necrosis Factor Alpha (TNF-α, catalog No. DTA00D, R&D Systems, Minneapolis, USA), Interleukin-1β (IL-1β, catalog No. MLB00C-1, R&D Systems, Minneapolis, USA), Interleukin-6 (IL-6, catalog No. D6050, R&D Systems, Minneapolis, USA), Nuclear Factor-kappa-light-chain-enhancer of activated B cells (NF-Kβ- p65, catalog No. MBS015549, MyBioSource, San Diego, USA), CASPASE-3 (catalog No. MBS018987, MyBioSource, San Diego, USA), Tissue carbonyl content (catalog No. MAK094 Sigma-Aldrich, Massachusetts, USA), NCAM, (catalog No. MBS2504405, MyBioSource, San Diego, USA) and GFAP, (catalog No., MyBioSource, San Diego, USA).

Western Blot

The total protein concentration in the brain and sciatic nerve was determined using the Bradford assay, a protein sample of 25 µg was combined with 4x Laemmli buffer. The mixture was then denaturation at a temperature of 95 °C for 5 minutes. Subsequently, the sample was separated using sodium dodecyl sulfate-polyacrylamide gel electrophoresis (SDS/PAGE) on a gel with a concentration of 12%; the separated components were de-posited onto a PDVF membrane. The membrane underwent a 2-hour blocking period, followed by incubation with primary antibodies diluted using a blocking buffer. Bax (Cat # MA5-14003, Thermo Fisher Scientific, CA, USA), Bcl2 (Cat. No.# MA5-11757, Thermo Fisher Scientific, CA, USA) Cox2 (Cat # 35–8200, Thermo Fisher Scientific, CA, USA), HO-1 (Cat. No.# MBS9144762, MyBioSource, ca, USA)., iNOS (Cat. No. # NBP2-80256, Novus Biologicals, LLC, USA)., Keap1 (Cat No #MBS714561, MyBioSource, Ca, USA), NF-κB (Cat. No.# PA5-29342, Thermo Fisher Scientific, CA, USA,), Nrf2 (Cat. No.# PA5-27882, Thermo Fisher, CA, USA), SOD2 (Cat. No.#: AF3419, Minneapolis, USA)., were incubated for 12 h at 4 °C with gentle shaking. The membrane was washed thrice using Tris-buffered saline supplemented with 1% Tween-20 (Sigma). Subsequently, the membranes were incubated with secondary antibodies (goat anti-rabbit IgG-HRP and goat anti-mouse IgG) at a dilution of 1:5000 for 1 hour at room temperature. Following three washes with Tris-buffered saline with 1% Tween-20, the protein bands of interest were seen and subjected to analysis using the ChemiDoc™ MP Imaging System (Bio-Rad, California, USA), by estimating the grayscale intensity of each band, and the intensity was normalized to the corresponding loading control (β-Actin) band intensity. The elative expression was calculated as fold changes compared to the control group. Data analysis was blindly conducted by independent biochemical specialist.

Statistical Analysis

The data acquired from the study were subjected to statistical analysis using SPSS 20.0 software. The data for all groups is presented as mean values ± standard errors of mean (SEM). The statistical analysis employed in this study for the biochemical measurements was conducted using one-way analysis of variance (ANOVA) followed by Tukey's post hoc testing to ascertain any significant variations between the different groups. Two-way ANOVA (treatment versus duration) followed by Bonferroni's post hoc test was used for data analyses of the behavioral tests.

Results

Chromatographic Analysis

After optimization, the ideal mobile phase comprised a 97:3 (v/v) mixture of sodium acetate buffer (100 mM, pH 3.5, containing 0.08% sodium dodecyl sulfate [SDS]) and propanol. Chromatographic separation was achieved under the following conditions: Column temperature maintained at 30 °C, flow rate of 0.8 mL/min, and Ultraviolet (UV) detection at 265 nm. The retention times for oxaliplatin and 5-Flu were 2.11 min and 5.48 min, respectively (Figure 1).

The method was validated according to ICH guidelines.[44] Calibration curves demonstrated linearity across concentration ranges of 0.3–100 µg/mL for oxaliplatin and 0.01–20 µg/mL for 5-Flu, with correlation coefficients (r^2) exceeding 0.999. Limits of detection (LOD) and quantification (LOQ) were determined as 0.38 µg/mL and 1.16 µg/mL for oxaliplatin, and 0.35 µg/mL and 1.08 µg/mL for 5-Flu (Table 1). Intraday and inter-day precision, expressed as relative

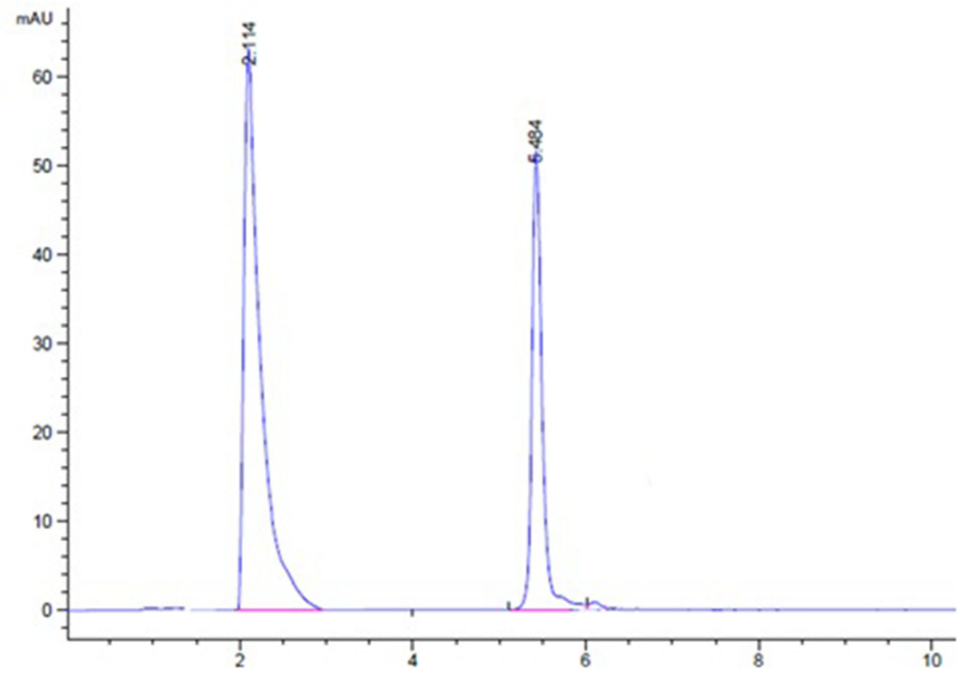

Figure 1 RP-HPLC chromatogram of 5-Flu and Oxaliplatin mixture at 265 nm.

standard deviation (RSD), were below 2%, while accuracy ranged from 99.12% to 101.45%, meeting ICH acceptance criteria (Table 1).

Effect on Rat's Body Weights

As shown in Figure 2A, the body weights of rats treated with oxaliplatin were determined weekly (weeks 0–6) and showed a gradual decline over the course of the experiment (145 g, 139 g, 137 g, 128 g, 130 g, 120 g, and 110 g, respectively), which was significantly lower compared to the control group. Similarly, intraperitoneal (i.p). administration of 5-Flu resulted in a slightly more pronounced weight loss than oxaliplatin alone (143 g, 130 g, 124 g, 111 g, 111 g, 103 g, and 95 g, respectively). The most significant weight reduction was observed in the group treated with both oxaliplatin and 5-Flu (142 g, 128 g, 113 g, 98 g, 96 g, 89 g, and 78 g, respectively). In contrast, the control group exhibited a steady increase in body weight over the same period (146 g, 171 g, 178 g, 189 g, 204 g, 211 g, and 236 g, respectively).

Table 1 The Validation of Intraday and Inter-Day Precision and Accuracy

Concentration (μg mL^{-1})	Precision (RSD%)		Accuracy (%)	
	Intraday	Inter-Day	Intraday	Inter-Day
5-Flu				
0.01	1.29	0.95	99.83	99.36
10	1.45	1.83	100.12	101.12
20	1.13	0.66	101.53	100.03
Oxaliplatin				
5	1.0	1.13	100.32	99.66
50	1.38	2.02	101.45	99.12
100	0.33	1.33	99.69	100.69

https://doi.org/10.2147/DDDT.S539603

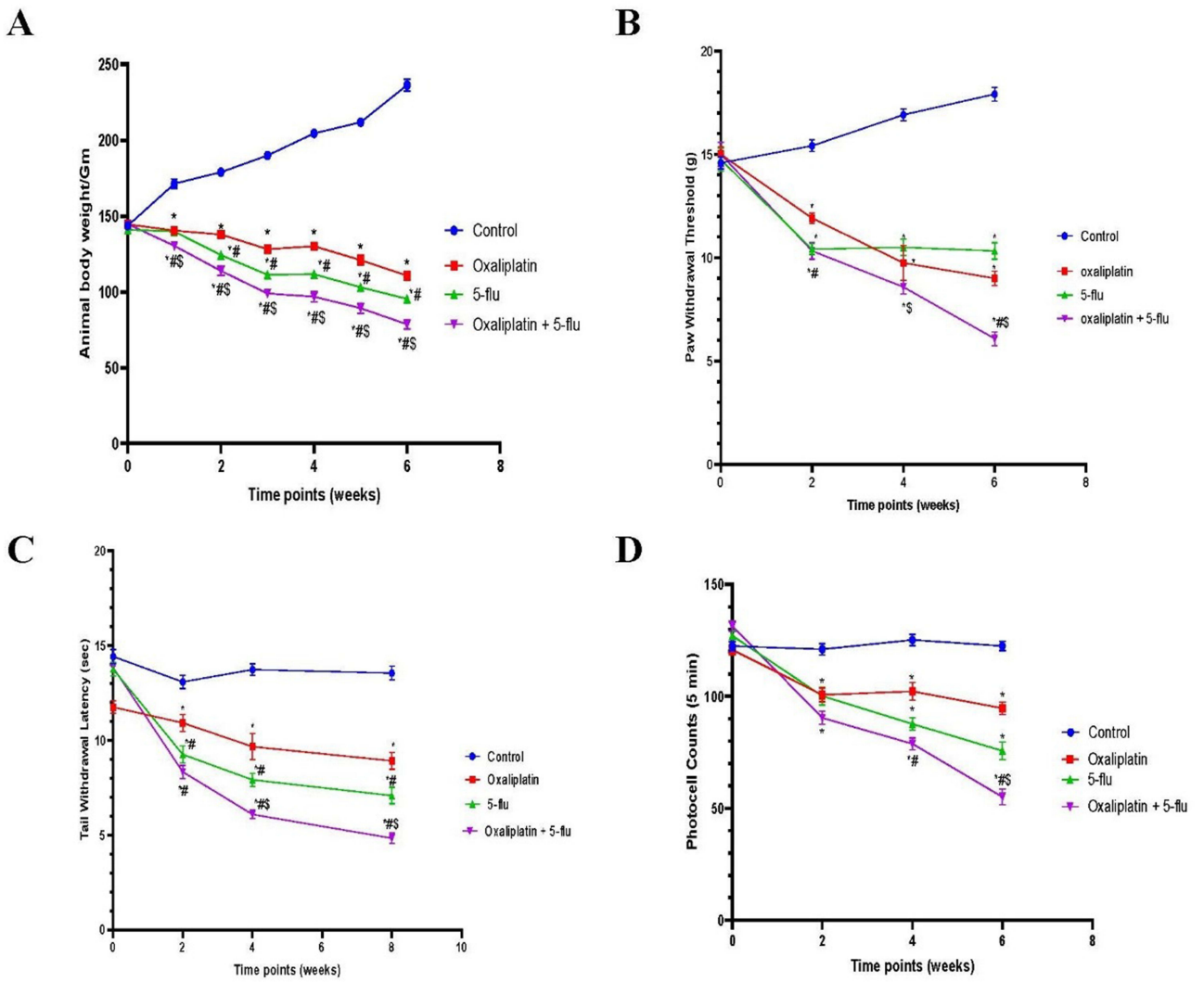

Figure 2 Effect of drug treatments on body weight and behavioral parameters. (**A**) body weights; (**B**) mechanical allodynia; (**C**) cold hyperalgesia; (**D**) locomotor activity; Results are represented as mean ± SEM. (n=12) (*) indicates significance compared to the normal control, (#) indicates significance compared to the oxaliplatin group, and ($) indicates significance compared to the 5-flu-treated group, at P <0.05.

Effect on Rats' Behavior

Mechanical Hyperalgesia

Rats were assessed for hyperalgesia bi-weekly at 0, 2, 4, and 6 weeks. Intraperitoneal (i.p). administration of oxaliplatin (6 mg/kg) induced significant mechanical hyperalgesia, as measured by the mechanical hyperalgesia test (14.7 g, 11.9 g, 10.5 g, and 10.3 g at 0, 2, 4, and 6 weeks, respectively; Figure 1). Similarly, i.p. administration of 5-Flu resulted in a mild but elevated hyperalgesic effect (14.5 g, 10.3 g, 9.25 g, and 9 g at the corresponding time points). Notably, the combined administration of oxaliplatin and 5-Flu produced the most pronounced hyperalgesic effect among all treated groups (14.9 g, 10 g, 8.5 g, and 6 g at 0, 2, 4, and 6 weeks, respectively) as shown in Figure 2B.

Effect on Tail-Immersion Test

The tail withdrawal latency test, a widely used method for assessing hyperalgesia in experimental animals, was employed in this study. Oxaliplatin treatment induced a significant and progressive reduction in tail withdrawal latency, with values of 13.8 sec, 10.9 sec, 9.6 sec, and 8.4 sec at 0, 2, 4, and 6 weeks, respectively. This reduction was more pronounced than that observed in the 5-Flu group, which recorded latencies of 13.5 sec, 9.25 sec, 7.9 sec, and 7.08 sec at the same time points. Furthermore, the combined administration of oxaliplatin and 5-Flu resulted in a marked decrease in tail

withdrawal latency, with values of 12 sec, 8.3 sec, 6.08 sec, and 4.9 sec at bi-weekly intervals, which were significantly lower than those of the control group (Figure 2C).

Effect on Locomotor Activity

Locomotor activity in rats was assessed bi-weekly at 0, 2, 4, and 6 weeks following the initiation of drug administration. Oxaliplatin administered intraperitoneally (i.p). induced a gradual and significant reduction in locomotor activity, with counts decreasing to 127, 100, 102, and 94 counts/5 min, compared to the control group (129, 121, 125, and 122 counts/5 min). Similarly, 5-Flu treatment resulted in decreased locomotor activity, with counts declining to 120, 100, 87, and 75 counts/5 min. Notably, the combined administration of oxaliplatin and 5-Flu led to a more pronounced reduction in locomotor activity, with counts dropping to 121, 90, 78, and 55 counts/5 min (Figure 2D).

Effect on the Cerebral Inflammatory Mediators

The expression of NF-kB (Figure 3A and C) and COX-2 (Figure 3B and D) in brain tissue was assessed using the Western blot technique, while the concentrations of TNF-α (Figure 3E), IL-6 (Figure 3F), and IL-1β (Figure 3G) in the brain were determined using ELISA. Results revealed a significant increase in the relative expression of NF-kB and COX-2, as well as elevated brain tissue concentrations of TNF-α, IL-6, and IL-1β, in both oxaliplatin-treated (NF-kB: 1.46 relative density; COX-2: 3.3 relative density; TNF-α: 7.9 pg/mg protein; IL-6: 10 pg/mg protein; IL-1β: 6.3 pg/mg

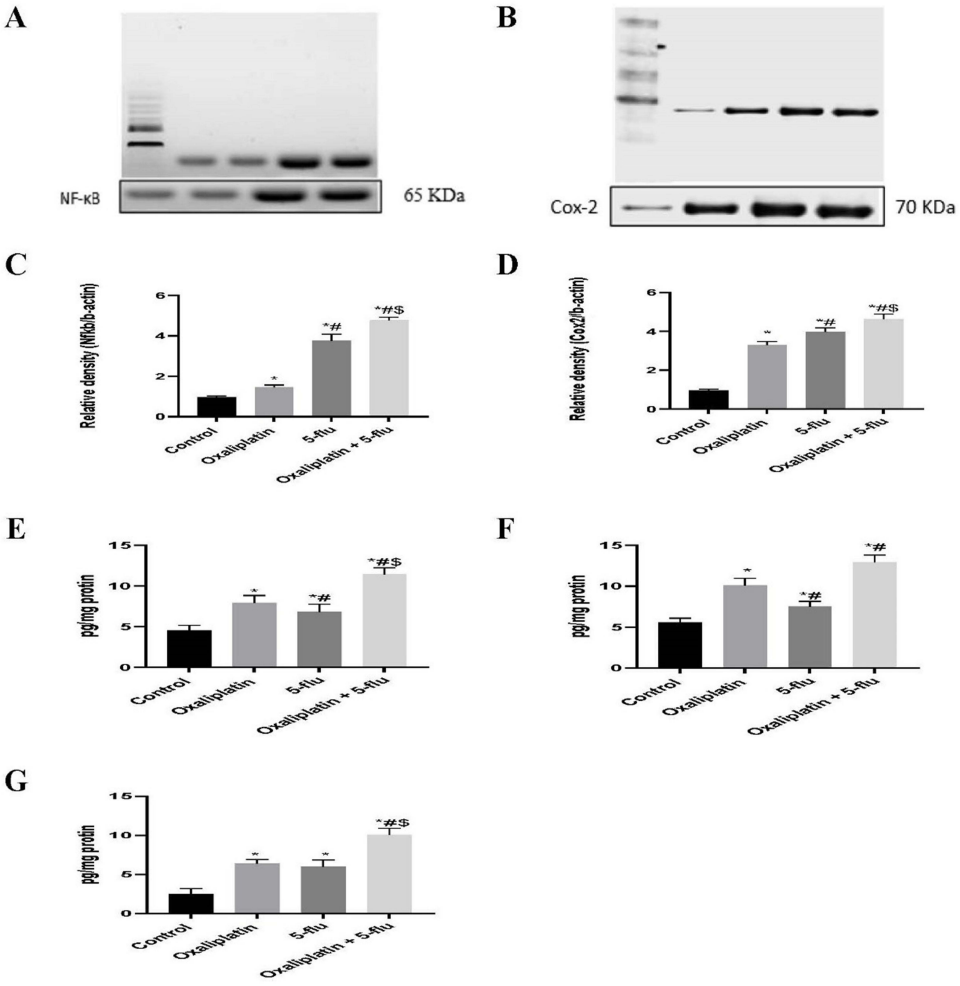

Figure 3 Effect of drug treatments on the cerebral inflammatory mediators. (**A**) Western blot analysis of NFκB; (**B**) Western blot analysis of COX-2; (**C**) Quantification of the levels of NFκB; (**D**) Quantification of the levels of COX-2 (**E**) Quantification of the levels of TNF-α; (**F**) Quantification of the levels of IL-6; (**G**) Quantification of the levels of IL-1β. Results are represented as mean ± SEM. (n=12) (*) indicates significance compared to the normal control, (#) indicates significance compared to the oxaliplatin group, and ($) indicates significance compared to the 5-flu-treated group, at $P < 0.05$.

https://doi.org/10.2147/DDDT.S539603

protein) and 5-Flu-treated groups (NF-kB: 3.75 relative density; COX-2: 3.98 relative density; TNF-α: 6.8 pg/mg protein; IL-6: 7.5 pg/mg protein; IL-1β: 6 pg/mg protein) compared to the control group. Notably, the highest levels of these inflammatory mediators were observed in the oxaliplatin + 5-Flu co-treated group (NF-kB: 4.76 relative density; COX-2: 4.64 relative density; TNF-α: 11.4 pg/mg protein; IL-6: 12.9 pg/mg protein; IL-1β: 10 pg/mg protein), which were significantly higher ($P < 0.05$) than those in the other treatment groups.

Effect on Cerebral Nitric Oxide

In this study, both nitric oxide (NO) concentration (Figure 4A) and inducible nitric oxide synthase (iNOS) expression (Figure 4B and D), were assessed in the brain tissue. Intraperitoneal (i.p). administration of oxaliplatin significantly increased NO levels to 2.7 µmol/g protein and iNOS expression to 1.8-fold relative to controls. In contrast, 5-Flu induced a more pronounced upregulation, with NO levels reaching 3.45 µmol/g protein and iNOS expression increasing to 2.8-fold. Notably, the combined administration of oxaliplatin and 5-Flu resulted in the highest NO concentration (5.7 µmol/g protein) and iNOS expression (5.2-fold) among all treatment groups.

Effect on Specific Neuronal Biomarker Damage

Both GFAP and NCAM are widely recognized biomarkers for assessing neuronal damage. Our findings revealed that the individual administration of oxaliplatin and 5-Flu significantly increased GFAP concentrations (Figure 4C) to 23.75 ng/mL and 28.4 ng/mL, respectively, and decreased NCAM levels (Figure 4E) to 9.75 ng/mL and 8.33 ng/mL, respectively,

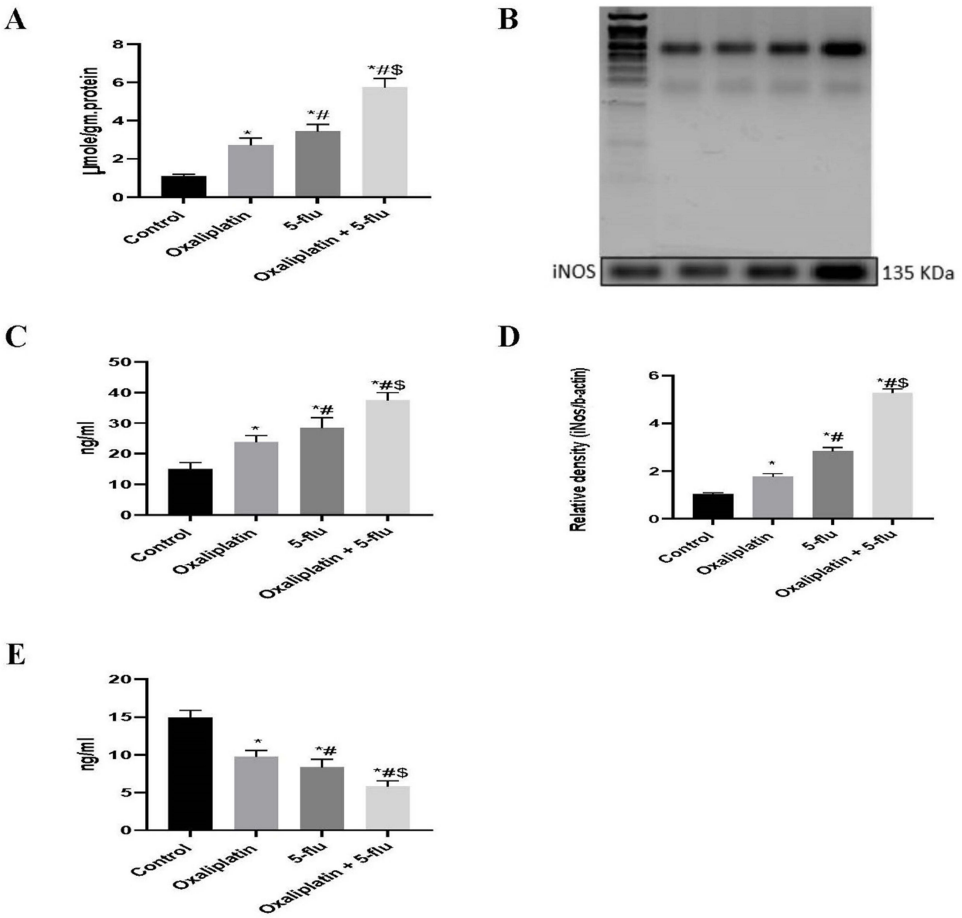

Figure 4 Effect of drug treatments on cerebral iNOS, NO, GFAB, and NCAM. (**A**) Quantification of the levels of nitric oxide; (**B**) Western blot analysis of inducible nitric oxide synthase; (**C**) Quantification of the levels of GFAP; (**D**) Quantification of the levels of iNOS; (**E**) Quantification of the levels of NCAM. Results are represented as mean ± SEM. (n=12) (*) indicates significance compared to the normal control, (#) indicates significance compared to the oxaliplatin group, and ($) indicates significance compared to the 5-flu-treated group, at $P < 0.05$.

compared to the control group (15 ng/mL for GFAP and 14.8 ng/mL for NCAM). Notably, the combined administration of the two drugs resulted in a more pronounced effect, elevating GFAP levels to 37.5 ng/mL and reducing NCAM concentrations to 5.8 ng/mL.

Effect on the Cerebral Apoptotic Bcl-2/ Bax/cCaspase-3 Pathway

To investigate the impact of the FOLFOX regimen on the Bcl-2/Bax/cCaspase-3 apoptotic pathway, the effects of oxaliplatin and 5-Flu were evaluated both individually and in combination. Oxaliplatin treatment moderately increased the relative expression of Bax (Figure 5B and D) and cCaspase-3 (Figure 5E and F) to 1.55 and 1.24, respectively, while decreasing Bcl-2 (Figure 5A and C) expression to 0.9. In contrast, intraperitoneal (i.p). administration of 5-Flu significantly elevated Bax and cCaspase-3 levels to 2.74 and 3.3, respectively, which were markedly higher than the effects observed with oxaliplatin alone. Additionally, Bcl-2 expression was reduced to 0.5 in the 5-Flu-treated group.

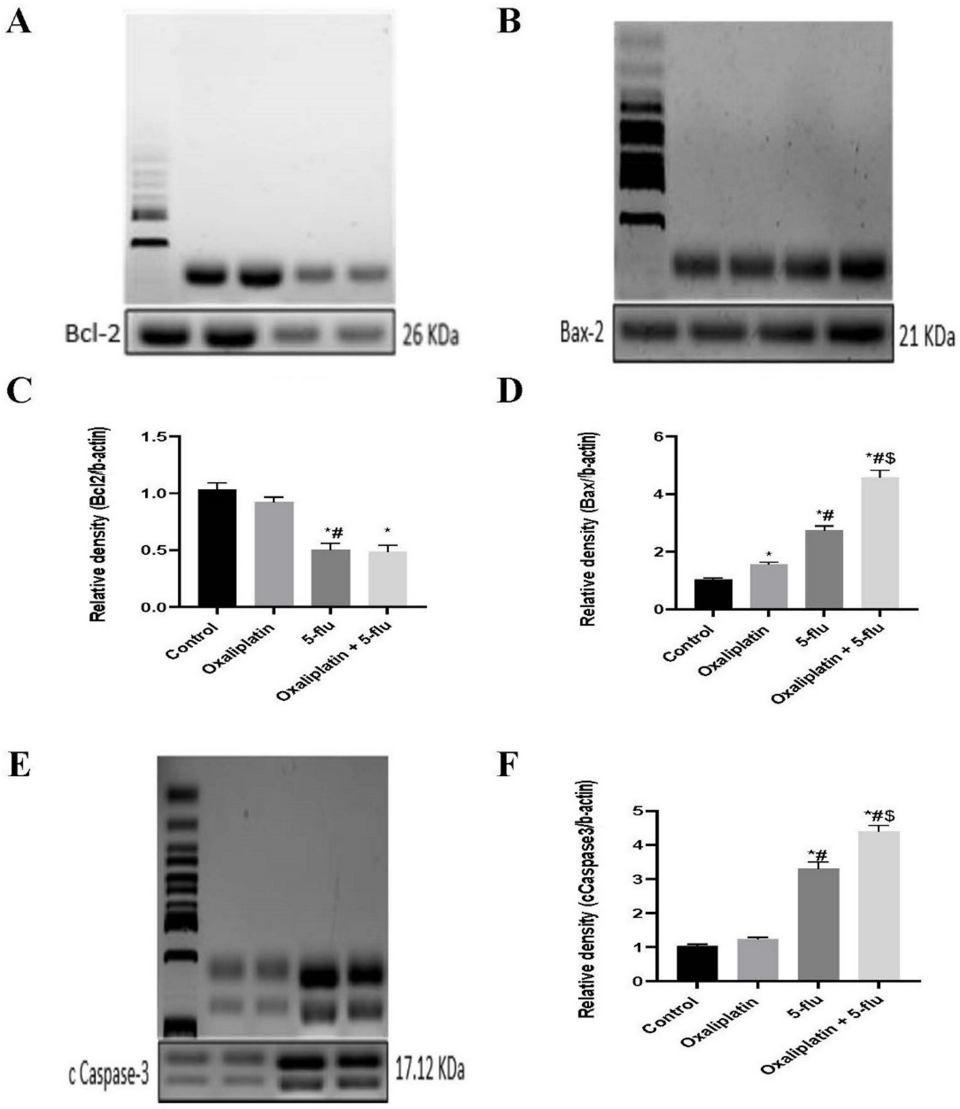

Figure 5 Effect of drug treatments on the apoptotic Bcl-2/ Bax/ cCaspase-3 pathway. (**A**) Western blot analysis of Bcl-2; (**B**) Western blot analysis of Bax-2; (**C**) Quantification of the levels of Bcl-2; (**D**) Quantification of the levels of Bax-2; (**E**) Quantification of the levels of cCaspase-3.Results are represented as mean ± SEM. (n=12) (*) indicates significance compared to the normal control, (#) indicates significance compared to the oxaliplatin group, and ($) indicates significance to the 5-flu-treated group, at P <0.05 compared.

https://doi.org/10.2147/DDDT.S539603

When administered together, the combination of oxaliplatin and 5-Flu further amplified the expression of Bax and cCaspase-3 to 4.57 and 4.4, respectively. However, the relative expression of Bcl-2 (0.48) in the combined treatment group did not differ significantly from that observed in the 5-Flu-treated group.

Effect on the Cerebral Antioxidant Enzymes

The neuronal system possesses robust intrinsic antioxidant defense mechanisms, including glutathione (GSH), glutathione peroxidase (GSH-Px), catalase, and SOD, which play critical roles in protecting the central nervous system (CNS) from oxidative stress damage. In this study, we investigated the impact of the FOLFOX regimen components on these antioxidant defenses. Our findings revealed that oxaliplatin significantly reduced the levels of GSH (Figure 6A), GSH-Px (Figure 6B), catalase (Figure 6C), and SOD (Figure 6D) to 4.7 nmol/mg protein, 349 U/mg protein, 24.3 U/mg protein, and 276.5 U/mg protein, respectively, compared to the control group (8.1 nmol/mg protein, 641 U/mg protein, 43.5 U/mg protein, and 380 U/mg protein). Similarly, 5-Flu decreased these parameters to 4.3 nmol/mg protein, 420 U/mg protein, 27.5 U/mg protein, and 303 U/mg protein, respectively. Notably, the combined administration of oxaliplatin and 5-Flu resulted in the lowest observed values (2.6 nmol/mg protein, 253 U/mg protein, 15.75 U/mg protein, and 221 U/mg protein, respectively).

Effect on the Cerebral Nrf-2 /SOD2 Pathway

The nuclear factor-erythroid 2-related factor 2 (Nrf2) pathway is a key regulator of cellular defense against oxidative stress. It controls the basal and inducible expression of numerous genes dependent on antioxidant response elements (AREs), playing a pivotal role in modulating the physiological and pathological effects of oxidant exposure. Using Western blot analysis, the relative expression levels of Nrf2 (Figure 7A and C), KEAP-1 (Figure 7B and D), and SOD2 (Figure 7E and F) in brain tissue were assessed. Oxaliplatin administration significantly reduced the relative expression of Nrf2 and SOD2 to 0.55 and 0.59 respectively, while increasing KEAP-1 expression to 2.1. Similarly, 5-Flu decreased the relative expression of Nrf2 and SOD2 to 0.48 and 0.60 respectively, and elevated KEAP-1 expression to 4.1. Notably, the combination of oxaliplatin and 5-Flu resulted in a more pronounced reduction in Nrf2 and SOD2, and a marked increase in KEAP-1 expression to 5.66 compared to the other treatment groups.

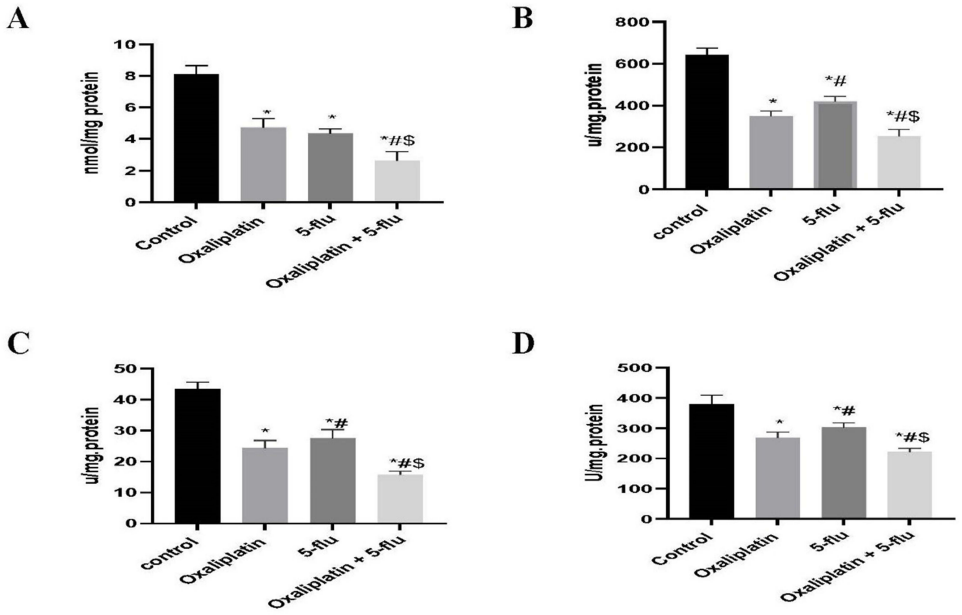

Figure 6 Effect of drug treatments on the cerebral antioxidant enzymes; GSH. GSH-Px, Catalase and SOD. (**A**) Quantification of the levels of GSH; (**B**) Quantification of the levels of GSH-Px; (**C**) Quantification of the levels of catalase; (**D**) Quantification of the levels of SOD. Results are represented as mean ± SEM. (n=12) (*) indicates significance compared to the normal control, (#) indicates significance compared to the oxaliplatin group, and ($) indicates significance compared to the 5-flu-treated group, at P <0.05.

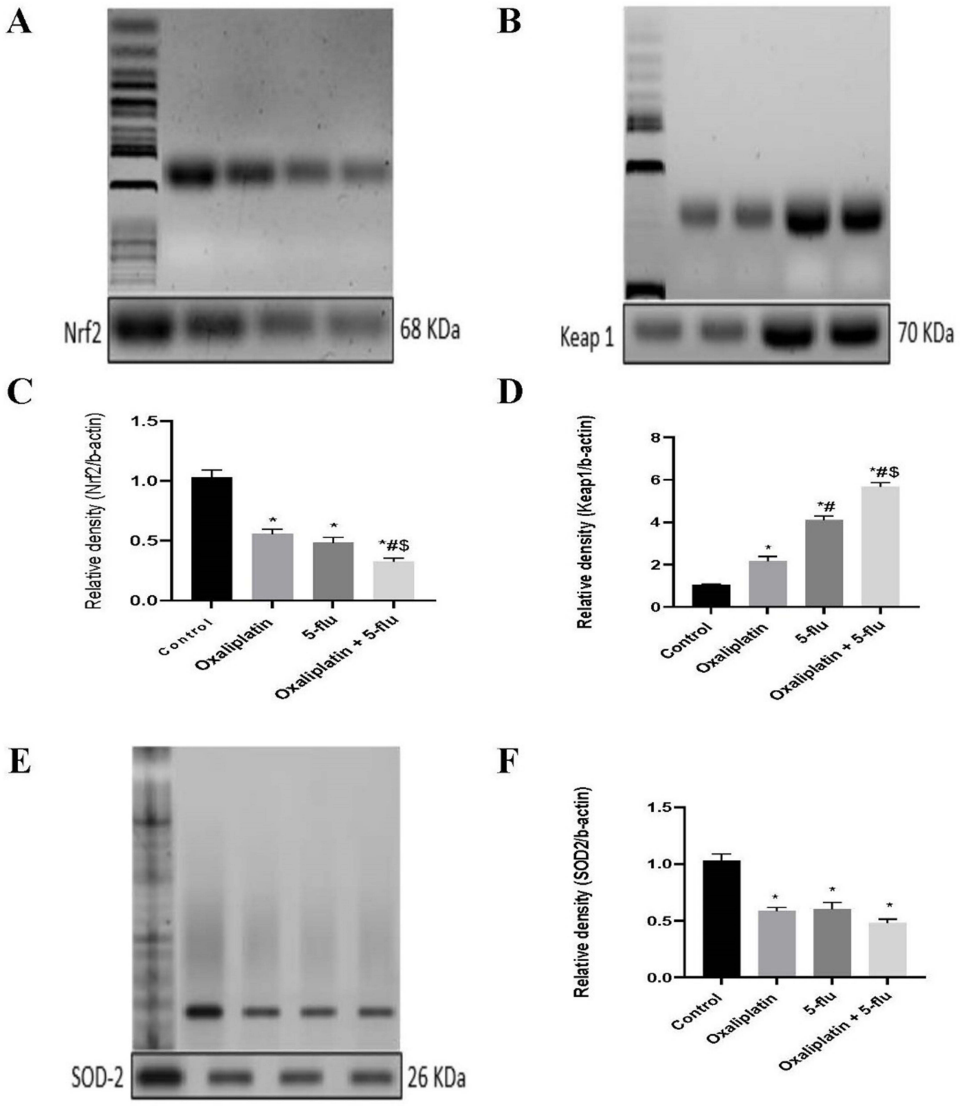

Figure 7 Effect of drug treatments on the cerebral Nrf-2 /HO-1 pathway. (**A**) Western blot analysis of Nrf-2; (**B**) Western blot analysis of Keap-1; (**C**) Quantification of the levels of Nrf-2; (**D**) Quantification of the levels of Keap-1; (**E**) Western blot analysis of SOD-2; (**F**) Quantification of the levels of SOD-2. Results are represented as mean ± SEM. (n=12) (*) indicates significance compared to the normal control, (#) indicates significance compared to the oxaliplatin group, and ($) indicates significance compared to the 5-flu-treated group, at P <0.05.

Effect on Cerebral Oxidative Stress Biomarkers

Malondialdehyde (MDA) and carbonyl tissue content are widely recognized biomarkers for assessing oxidative stress-induced tissue damage. In this study, we measured MDA, tissue carbonyl content, and TAC in the cerebral tissue. Oxaliplatin administration significantly elevated carbonyl content (Figure 8A), and MDA (Figure 8B) levels in the cerebral tissue to 2.09 nmol/mg protein and 2.25 nmol/mg protein respectively. Meanwhile, TAC (Figure 8C) was significantly reduced in the brain tissue compared to the control group (1.16 U/mg. protein). Similarly, the 5-Flu treated group exhibited significantly higher carbonyl content and MDA levels in the brain tissue (4.5 nmol/mg protein and 2 nmol/mg protein, respectively), alongside significantly lower TAC (1.3 U/mg. protein). Notably, in the brain tissue, oxaliplatin + 5-Flu treated group demonstrated the highest levels of carbonyl content and MDA (6.8 nmol/mg protein and 2.7 nmol/mg protein, respectively) and the lowest TAC (0.98 U/mg protein) among all treated groups.

https://doi.org/10.2147/DDDT.S539603

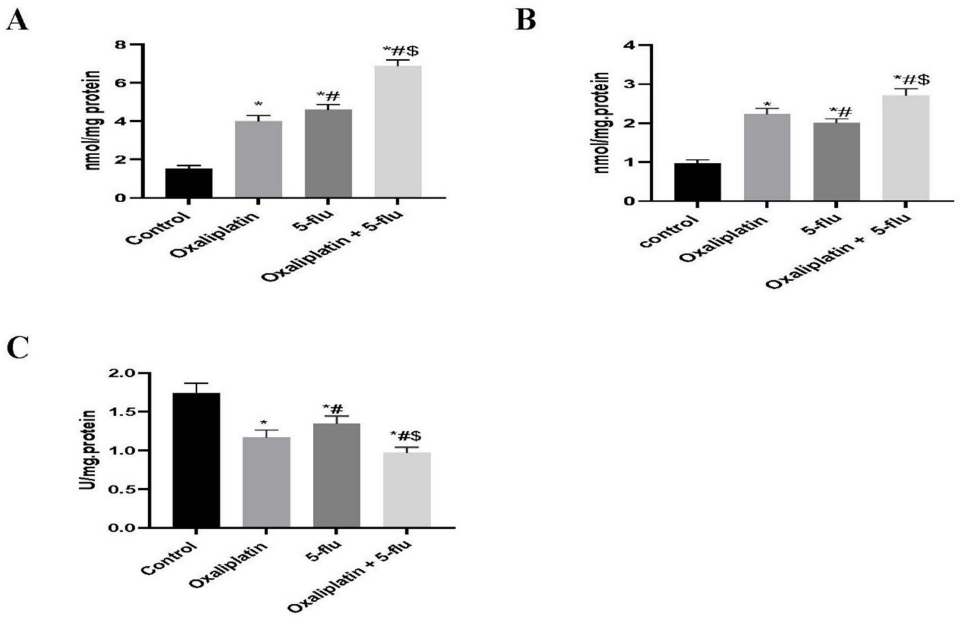

Figure 8 Effect of drug treatments on cerebral tissue Carbonyl content, MDA, and TAC. (**A**) Quantification of the levels of Carbonyl contents; (**B**) Quantification of the levels of MDA; (**C**) Quantification of the levels of TAC. Results are represented as mean ± SEM. (n=12) (*) indicates significance compared to the normal control, (#) indicates significance compared to the oxaliplatin group, and ($) indicates significance compared to the 5-flu-treated group, at P <0.05.

Effect on Sciatic Nerve Inflammatory and Oxidative Stress Biomarkers

In this study, tissue carbonyl content, GSH, TAC, MDA, and TNF-α were determined in the sciatic nerve. Regarding tissue carbonyl content, both oxaliplatin and 5-Flu produced a significant upregulation (1.05 and 1.01 nmol/mg protein, respectively) that was significantly augmented by the combined administration of both drugs (1.61 nmol/mg protein), as shown in Figure 9A. On the other hand, the GSH contents of the sciatic nerve in oxaliplatin (3.21 nmol/ mg protein) and 5-Flu (3.02 nmol/ mg protein) treated groups were found significantly lower than control group, while the combined administration of both drugs produced a significantly (P <0.05) further reduction (1.94 nmole/ mg protein) compared to their individual administration as shown in Figure 9B.

As shown in Figure 9C, the sciatic TAC was significantly decreased by oxaliplatin (0.44 U/mg protein) and 5-Flu (0.42 U/mg protein) administration compared to the control group, while the TAC was found 0.33 U/mg protein at oxaliplatin + 5-Flu treated group. Furthermore, sciatic nerve content of MDA (Figure 9D) was significantly upregulated by the combined administration of oxaliplatin + 5-Flu to 2.2 nmol/mg protein compared to the control group, which was significantly higher than oxaliplatin (1.6 nmol/mg protein) and 5-Flu (1.7 nmol/mg protein) individual administration.

Regarding the effect of our investigational drugs on the sciatic nerve content of TNF-α, we found a significant (P < 0.05) increase in its concentrations in both oxaliplatin (5.11 pg/mg protein) and 5-Flu (4.08 pg/mg protein) treated groups compared to the control group. In comparison, the highest level of TNF-α concentrations was detected in the Oxaliplatin + 5-Flu treated group (6.8 pg/mg protein), as shown in Figure 9E.

Histopathological Results

As illustrated in Figure 10, a histopathological examination of the cerebral cortex in the normal control group revealed a typical, intact cortical structure. In contrast, sections from oxaliplatin-treated rats exhibited thickened and congested blood vessels, increased fibrotic tissue, edema, and pronounced neuronal vacuolation. Similarly, the 5-Flu-treated group displayed moderately thickened and congested blood vessels, accompanied by small blood vessel hemorrhage, a marked increase in fibrotic tissue, edema, and neuronal vacuolation compared to the oxaliplatin group. Furthermore, cerebral cortex tissues from

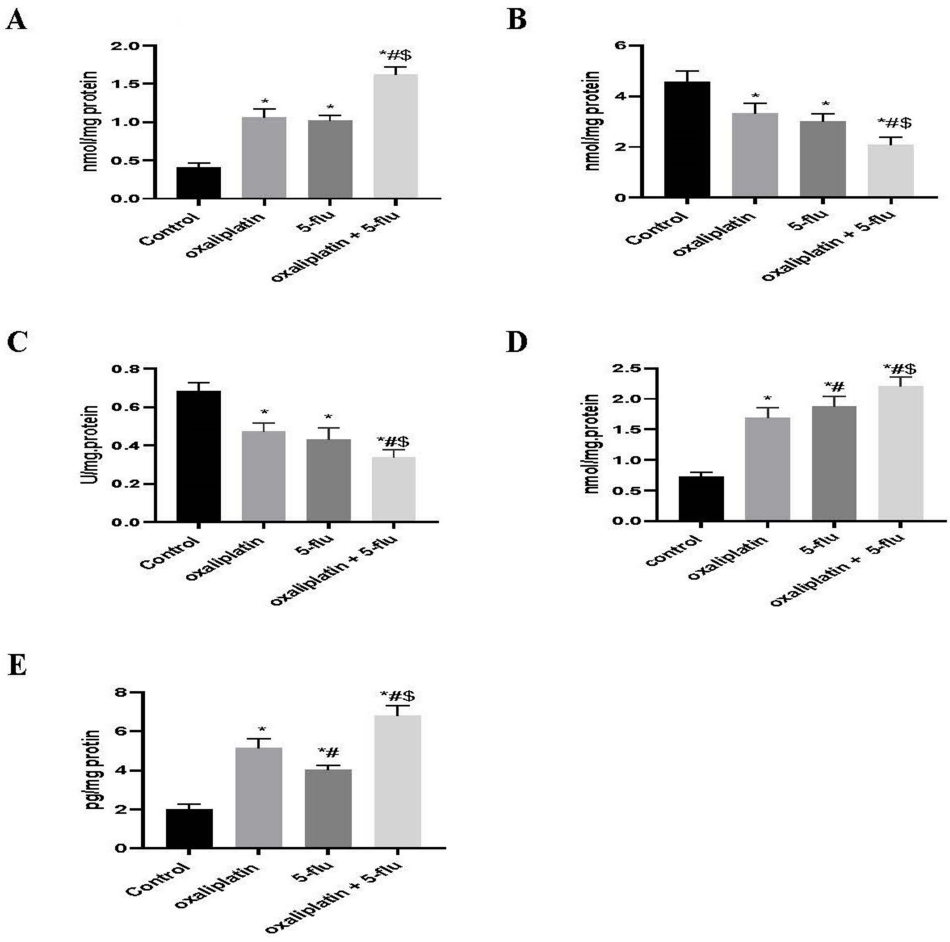

Figure 9 Effect of drug treatments on sciatic nerve inflammatory, oxidative stress, and tissue damage biomarkers. (**A**) Quantification of the levels of Carbonyl contents; (**B**) Quantification of the levels of GSH; (**C**) Quantification of the levels of TAC; (**D**) Quantification of the levels of MDA; (**E**) Quantification of the levels of TNF-α. Results are represented as mean ± SEM. (n=12) (*) indicates significance compared to the normal control, (#) indicates significance compared to the oxaliplatin group, and ($) indicates significance compared to the 5-flu-treated group, at P <0.05.

the oxaliplatin + 5-Flu group showed small areas of necrotic tissue, neuronal edema, and congested blood vessels, with these changes being significantly more severe than those observed in the oxaliplatin and 5-Flu groups alone.

As illustrated in Figure 11, a histopathological examination of the cerebellum in the normal control group revealed a typical cerebellar structure with intact Purkinje fibers, molecular layers, and granular layers. In contrast, cerebellar tissues from the oxaliplatin-treated group exhibited moderate necrosis of Purkinje fibers, accompanied by congested blood vessels and an infiltration of inflammatory cells. Similarly, sections from the 5-Flu-treated group displayed moderately congested blood vessels, mild edema, and scattered necrotic Purkinje fibers. Likewise, the oxaliplatin + 5-Flu group showed extensive degeneration of Purkinje fibers, hemorrhagic small blood vessels, edema, and an infiltration of inflammatory cells.

As illustrated in Figure 12, a histopathological examination of sciatic nerve fibers in the normal control group revealed a typical nerve fiber structure with no signs of inflammation or neuronal degeneration. In contrast, nerve sections from the oxaliplatin-treated group exhibited moderate inflammatory changes accompanied by axonal lipid alterations. Similarly, the 5-Flu-treated group displayed degenerative inflammatory changes and focal areas of nerve demyelination. Notably, nerve sections from the oxaliplatin + 5-Flu-treated group demonstrated advanced neuronal demyelination, axonal degeneration, pronounced inflammation, and nerve fiber swelling.

https://doi.org/10.2147/DDDT.S539603

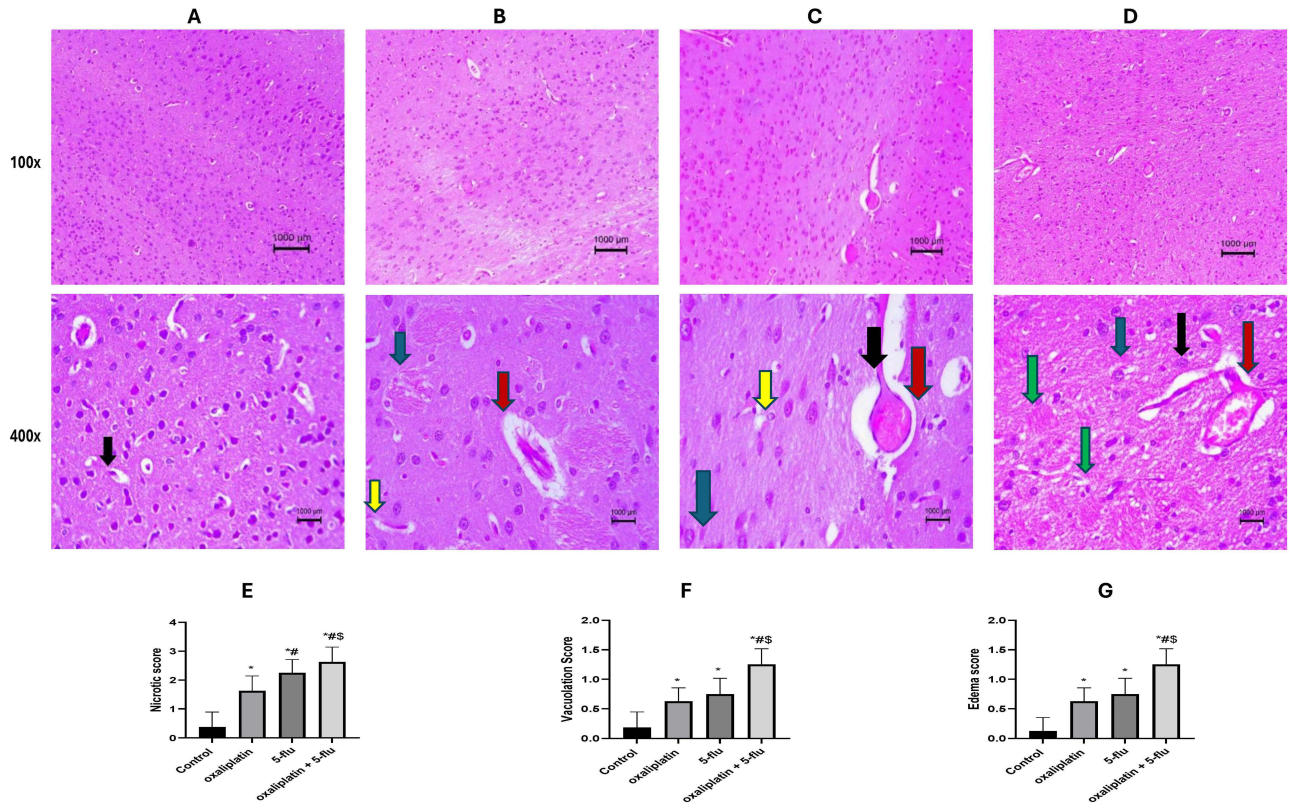

Figure 10 Representative histopathological image of rat's Cerebral cortex using H&E stain at 100x and 400x magnification. (**A**) Control normal group, showing a normal structure of the cerebral cortex; (**B**) Oxaliplatin group, showing thickened and congested blood vessels (**C**) 5-flu group, showing moderate thickened and congested blood vessels associated with small blood vessel hemorrhage, (**D**) oxaliplatin + 5-flu group, (**E**) Quantification of necrotic changes, (**F**) Quantification of neuronal vacuolation, (**G**) Neuronal edema quantification, showing small necrotic tissue and neuronal edema associated with congested blood vessels. Black arrow point to dilated blood vessel, Yellow arrow point to dilated and congested blood vessel, Blue arrow point to degenerative changes, Green arrow point to inflammatory changes, and Red arrow point to dilated and neuronal edema. Results are represented as mean ± SEM. (n = 6). (*) indicates significance compared to the normal control, (#) indicates significance compared to the oxaliplatin group, and ($) indicates significance compared to the 5-flu-treated group, at P <0.05.

Discussion

Cancer represents one of the most significant societal, public health, and economic challenges of the 21st century. It accounts for approximately one in six deaths globally (16.8%) and one in four fatalities attributed to noncommunicable diseases (NCDs) (22.8%).[45] Chemotherapy remains a cornerstone of cancer treatment, and its efficacy well-established since the 1960s, leading to substantial improvements in clinical outcomes. However, a major limitation of chemotherapy is its propensity to induce unintended adverse effects in non-cancerous tissues, resulting in cardiovascular, neurological, skeletal, and other systemic morbidities.

Oxaliplatin, in combination with 5-Flu, is a cornerstone of colorectal cancer treatment, forming the basis of the FOLFOX regimen.[46] While 5-Flu monotherapy achieves a modest response rate of approximately 20% in metastatic colorectal cancer, its combination with oxaliplatin significantly improves therapeutic outcomes.[47] However, research on the toxicity of this regimen, particularly its effects on the CNS, remains limited. Neurotoxicity is a major dose-limiting side effect of FOLFOX, yet the mechanisms underlying FOLFOX-induced neurotoxicity are poorly understood, and effective strategies to prevent or treat this complication are lacking. Addressing this gap, the current study explores the molecular mechanisms through which oxaliplatin and 5-Flu, the key components of FOLFOX, induce neurotoxicity in the brain and sciatic nerve, aiming to inform the development of preventive and therapeutic interventions.

Mobile phase conditions for HPLC separations were systematically adjusted to obtain sharp, symmetrical, and well-resolved peaks. After testing different compositions and ratios, the optimal system consisted of 3% propanol and 97% acetate buffer (pH 3.5) containing 0.08% SDS, with the column temperature set to 30°C. The method exhibited excellent recovery (>99%) and precision, with intraday and inter-day RSD% (under 2%), fulfilling predefined validation standards.

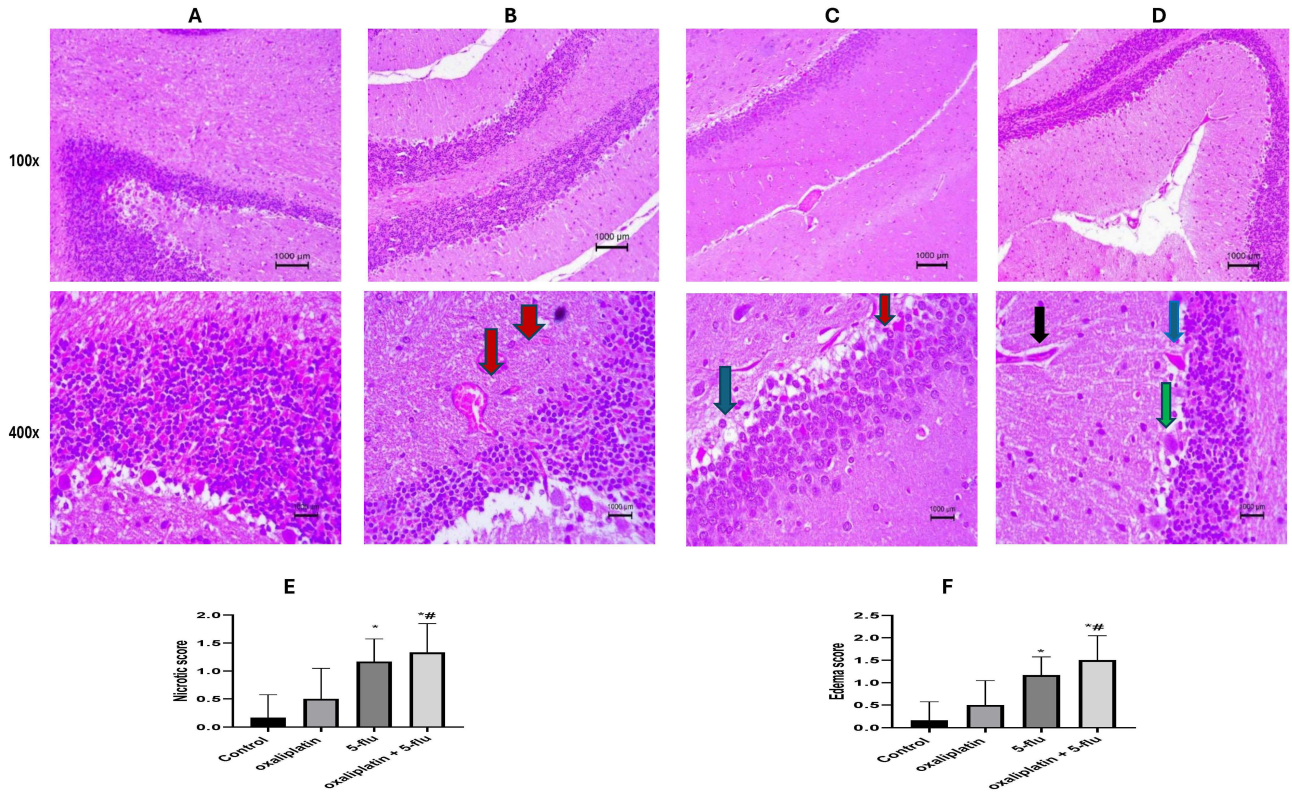

Figure 11 Representative histopathological image of rats Cerebellum using H&E stain at 100x and 400x magnification. (**A**) Control normal group, showing normal structure of cerebellum with normal Purkinje fibers, molecular and granular layer, (**B**) oxaliplatin group, showing moderate necrotic Purkinje fibers associated with congested blood vessels and inflammatory cells infiltration. (**C**) 5-flu group, showing moderately congested blood vessels, mild edema, and scattered necrotic Purkinje fibers; (**D**) oxaliplatin + 5-flu group, (**E**) Quantification of necrotic changes, (**F**) Neuronal edema quantification, showing widely scattered degenerated Purkinje fibers, hemorrhagic small blood vessels, and edema associated with inflammatory cells infiltration. Black arrow point to dilated blood vessel, Blue arrow point to degenerative changes, Green arrow point to inflammatory changes, and Red arrow point to dilated and neuronal edema. Results are represented as mean ± SEM. (n = 6). (*) indicates significance compared to the normal control, and (#) indicates significance compared to the oxaliplatin group at P <0.05.

Accuracy assessments confirmed reliability, showing deviations within ±3% of target concentrations. A UV absorbance detector was selected for quantification due to its affordability and widespread adoption in pharmaceutical settings. This approach provided robust analyte measurement without requiring prior sample derivatization.

Under normal physiological conditions, oxaliplatin and 5-Flu are undetectable in brain tissues due to the protective blood-brain barrier (BBB). However, administration of the FOLFOX regimen induces inflammation, which compromises the BBB and facilitates penetration of both drugs into brain tissues. The HPLC method was employed to quantify oxaliplatin and 5-Flu in brain homogenates. Results revealed significantly higher concentrations of oxaliplatin (0.66 ± 0.91 µg/mL) and 5-Flu (2.7 ± 1.76 µg/mL) in the combined FOLFOX group compared to the oxaliplatin monotherapy group (0.509 ± 0.12 µg/mL) and 5-Flu monotherapy group (0.74 ± 0.03 µg/mL). These findings suggest synergistic neurotoxic effects arising from the co-administration of both drugs.

Behavioral assessments evaluating diverse sensory dimensions of neuropathic pain were conducted both before and after drug administration. In clinical settings, adverse neurological symptoms, such as acute cold allodynia accompanied by paresthesia and hypoesthesia, often necessitate treatment discontinuation.[48] Our results demonstrated that the co-administration of oxaliplatin and 5-Flu significantly lowered the pain threshold, as measured through behavioral tests, including tail-immersion, paw pressure, and locomotor activity assessments. These specific nociceptive behavioral markers closely mirror symptoms observed in cancer patients, suggesting the presence of advanced neuroinflammatory processes.

Oxidative stress is widely recognized as a key contributor to neuronal damage in various neuropathy models, such as diabetic neuropathy, acrylamide-induced neuropathy, and chemotherapy-induced neuropathy.[40,49] While antineoplastic

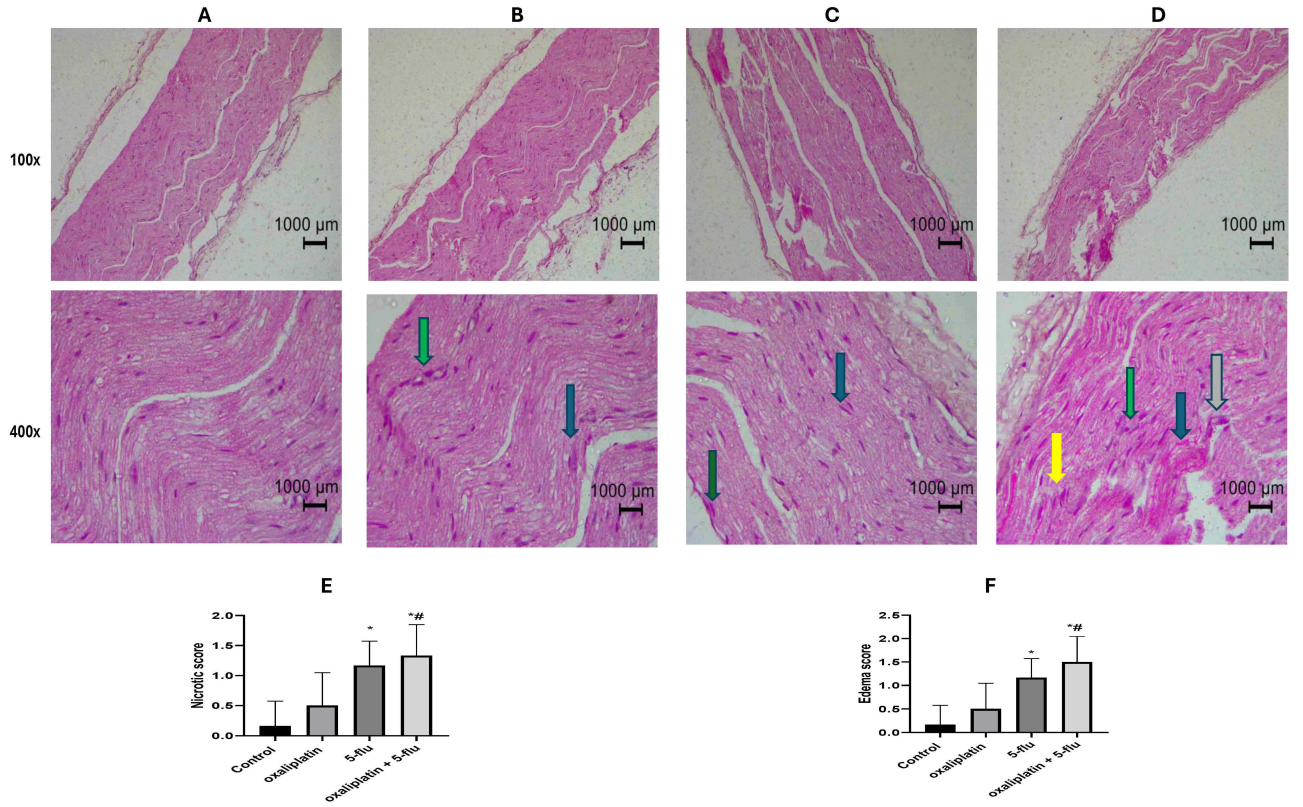

Figure 12 Representative histopathological image of rat's sciatic nerve fiber using H&E stain at 100x and 400x magnification; (**A**) Control normal group, showing normal structure of sciatic nerve without any inflammatory or neuronal degeneration (**B**) oxaliplatin group, showing moderate inflammatory changes with axonal lipoid changes. (**C**) 5-flu group, showing degenerative inflammatory changes and nerve demyelination in some areas (**D**) oxaliplatin + 5-flu group, (**E**) Quantification of necrotic changes, (**F**) Neuronal edema quantification, showing advanced neuronal demyelination, axonal degeneration, prominent inflammation, and nerve fiber swelling. Gray arrow point to fibrotic changes, Yellow arrow point to dilated and congested blood vessel, Blue arrow point to degenerative changes, Green arrow point to inflammatory changes, Red arrow point to dilated and neuronal edema. Results are represented as mean ± SEM. (n = 6). (*) indicates significance compared to the normal control, and (#) indicates significance compared to the oxaliplatin group at P <0.05.

drugs generate ROS to induce apoptosis in cancer cells, the same ROS can adversely affect neuronal cells, leading to chemotherapy-induced neurotoxicity. Oxidative stress-induced neurodegeneration can arise through multiple mechanisms, including depletion of antioxidant defenses, biomolecular damage, demyelination, neuroinflammation, and neuronal apoptosis.[50] In this study, tissue carbonyl content and malondialdehyde (MDA) levels in both the brain and sciatic nerve were significantly elevated following individual administration of oxaliplatin and 5-Flu. Notably, combined administration of the two drugs resulted in a further increase in these markers, suggesting a synergistic pro-oxidant effect on the CNS. Additionally, the levels of key endogenous antioxidants were assessed, revealing a dramatic reduction in cerebral tissue concentrations of catalase, SOD, glutathione peroxidase (GSH-Px), and reduced glutathione (GSH). A significant depletion of GSH was also observed in the sciatic nerve. These findings, supported by TAC measurements, confirm the presence of advanced oxidative stress in neuronal tissues.

Nuclear factor-erythroid 2-related factor 2 (Nrf2), a key transcription factor, plays a critical role in maintaining mitochondrial homeostasis. Pharmacological and genetic studies suggest a regulatory interplay between Nrf2 and nuclear factor-kappa B (NF-κB), where Nrf2 deficiency may exacerbate NF-κB activation, leading to increased cytokine production.[51,52] Nrf2 knockout mice demonstrate heightened susceptibility to oxidative stress-induced chemical toxicity and disease progression, highlighting the importance of Nrf2 in cellular defense mechanisms. These findings have led researchers to propose that enhancing Nrf2's protective effects against oxidative stress and mitochondrial dysfunction could offer a promising therapeutic strategy for alleviating neuropathic pain.[53,54]

Under normal physiological conditions, Nrf2 is bound to Kelch-like ECH-associated protein 1 (Keap1) in the cytoplasm.[55] However, under oxidative or stressful conditions, Nrf2 dissociates from Keap1 and translocates to the

nucleus, where it forms a heterodimer with MAF proteins. This Nrf2–MAF complex binds to ARE, initiating the transcription of cytoprotective genes such as heme oxygenase-1 (HO-1), NADPH, SOD, glutathione cysteine ligase, glutathione S-transferases, and catalase.[56–58] Among these, HO-1 and its byproducts play a critical role in mitigating oxidative stress, regulating apoptosis, modulating inflammation, and promoting angiogenesis.[59] In this study, Western blot analysis revealed a significant downregulation of Nrf2 and SOD2 protein levels in the cerebral tissues of animal groups treated with oxaliplatin or 5-Flu individually. This effect was more pronounced in the group receiving combined oxaliplatin and 5-Flu treatment. Conversely, Keap1 levels were markedly elevated in the cerebral tissues of all treated groups, with the highest concentrations observed in the oxaliplatin + 5-Flu group. These findings suggest that FOLFOX-induced neurotoxicity may be mediated, in part, by the disruption of the Nrf2-Keap1 antioxidant pathway and the subsequent impairment of cellular defense mechanisms.

In addition to its impact on proliferating immune cells, chemotherapy can modulate various components of the immune system, such as cytokine production and intracellular signaling pathways in immune cells, potentially leading to neuroinflammation and sensitization of the sensory nervous system.[60,61] Neuroinflammatory responses are driven by key pro-inflammatory cytokines (*eg*, IL-1β, IL-6, and TNF-α), chemokines, secondary messengers (*eg*, NO and prostaglandins), and ROS.[62,63] This study demonstrated that i.p. administration of oxaliplatin combined with 5- 5-Flu significantly increased cerebral levels of inflammatory mediators, including NF-κB, COX2, TNF-α, IL-1β, and IL-6. Notably, 5-Flu exhibited a stronger upregulatory effect on NF-κB and COX2 compared to oxaliplatin, whereas oxaliplatin had a more pronounced stimulatory effect on cerebral TNF-α and IL-6 levels than 5-Flu.

GFAP, a type III intermediate filament, serves as a specific biomarker for astrocytes and is essential for maintaining cytoskeletal stability and supporting neuronal function.[64,65] Notably, GFAP expression is significantly upregulated in response to various neurological injuries,[66] and Its gene expression is primarily regulated by nuclear factor κB signaling.[67] Abnormal GFAP expression is implicated in a range of neuropathologies, including neuroinflammation, neurodegeneration, cerebral edema, and traumatic brain injury. Conversely, NCAM, a member of the immunoglobulin superfamily, is a membrane-associated protein crucial for nervous system development. It modulates neuronal migration, neurite outgrowth, synapse formation, and synaptic plasticity.[68] Beyond its role in neural development, NCAM participates in myogenesis and nerve and muscle tissue regeneration,[69] As a key cell adhesion molecule, NCAM's involvement in cell migration, neurite outgrowth, and synaptic plasticity is well-established.[70,71] Notably, both increases and decreases in NCAM levels have been associated with diverse neurological diseases, highlighting that disruptions in its homeostatic balance, rather than absolute levels, are likely critical factors.[69,72]

In this study, we employed the ELISA technique to assess cerebral concentrations of GFAP and NCAM proteins. The results revealed a significant upregulation of GFAP alongside a marked downregulation of NCAM across all treated groups. Notably, the combined administration of oxaliplatin and 5-Flu demonstrated a pronounced synergistic effect on these protein expression patterns.

Mitochondria-mediated apoptosis, a critical process in neuronal programmed cell death, is largely governed by the B-cell lymphoma 2 (Bcl-2) protein family.[73] This family consists of both pro-apoptotic members, such as Bax, and anti-apoptotic members. The balance between these opposing forces dictates the release of apoptogenic factors from mitochondria. Specifically, pro-apoptotic proteins promote this release, while anti-apoptotic proteins inhibit it.[74,75]

The role of Bcl-2 in neuronal survival has been extensively studied. For instance, in vitro models of trophic factor withdrawal, which induce programmed cell death in neuronal cell lines and primary neurons, demonstrate that Bcl-2 overexpression effectively prevents apoptosis.[74,76] Similarly, in vivo studies using transgenic mice show that Bcl-2 overexpression enhances neuronal populations across various brain regions by suppressing endogenous apoptosis.[77,78]

Mechanistically, it is understood that pro-apoptotic Bcl-2 family members facilitate, and anti-apoptotic members impede, the release of cytochrome c into the cytosol. This release triggers the activation of caspases, notably caspase-9 and caspase-3, culminating in apoptosis.[74,76] Caspases, a family of proteases, are central mediators of both intrinsic and extrinsic apoptotic pathways.[79] Furthermore, Bax plays a pivotal role in regulating neuronal cell death. Elevated Bax expression promotes the formation of Bax homo- or heterodimers with Bcl-2, ultimately contributing to cerebral cell apoptosis.[80]

Scientists have found that oxidative stress is a major trigger of apoptosis by damaging cellular components and activating signaling pathways that lead to programmed cell death,[81,82] as ROS production during oxidative stress leads to mitochondrial dysfunction, release of pro-apoptotic factors (*eg*, cytochrome c), and activation of caspases that execute apoptosis.[83] Moreover, oxidative stress influences apoptosis through modulation of factors like NF-κB, p53, and Bcl-2 family proteins, further supporting its role as an initiator rather than a result of apoptosis.[84]

Our findings demonstrate that 5-Flu elicits a substantially stronger oxidative as previously mentioned and pro-apoptotic response than oxaliplatin. Specifically, 5-Flu induced a pronounced upregulation of cerebral caspase-3 and Bax, accompanied by a significant downregulation of Bcl-2. In contrast, oxaliplatin produced a less pronounced effect on these markers. Importantly, the combined administration of 5-Flu and oxaliplatin resulted in a synergistic increase in pro-apoptotic activity. This suggests that the potentiation of the Bax/caspase-3 pro-apoptotic pathway, along with the reduction of the anti-apoptotic protein Bcl-2 in cerebral tissue, plays a pivotal role in the neurotoxicity induced by the FOLFOX regimen.

The demonstrated oxidative stress, apoptosis, and inflammation induced by oxaliplatin and 5-fluorouracil, especially in combination, provide mechanistic insights relevant to chemotherapy-induced neurotoxicity observed in patients. The validated HPLC method for brain drug quantification offers a model for assessing drug penetration and accumulation within the human CNS, which is crucial for understanding dose-dependent neurotoxic effects. Behavioral and histo-pathological parallels, such as neuronal damage and reduced pain thresholds in rats, can be correlated with clinical symptoms like neuropathic pain and cognitive dysfunction in cancer patients. However, human translation requires dose scaling, assessment of BBB permeability differences, and confirmation through clinical neurotoxicity biomarker studies. Ultimately, this preclinical data supports the development of targeted interventions to mitigate neurotoxic side effects of these chemotherapeutic agents and guides monitoring strategies to improve patient outcomes during combination chemotherapy regimens.

Study Limitations

Despite the importance of the present study and its findings, its essential to address its limitations that can help in the improvement of future works; the investigated drugs needs to be examined on the human for toxicity conformation, hence rats and humans can differ significantly in drugs pharmacokinetics, the drug dosages toxicity in rats are not always directly predictive for humans, and metabolic rates may require species-specific adjustments rather than simple body weight conversions. More different doses of both oxaliplatin and 5-Flu needs to be examined to determine the exact toxic dose, and the duration of the experiment needs to be extended to examine the effect of tested drugs on the long run, finally using computed tomography and magnetic resonance scan can determine the exact affected areas in the brain.

Conclusions

This study revealed that FOLFOX can induce neurotoxicity via; pro-inflammatory (COX-II, TNF-α, IL-6, and NF-κβ upregulation), pro-apoptotic (caspase-3 and Bax upregulation, and Bcl-2 depletion), and pro-oxidant (Nrf-2 and SOD2 downregulation) pathways. Moreover, this study introduced a newly developed method for the determination of 5-Flu and oxaliplatin cerebral concentrations using HPLC, providing critical insights into developing therapeutic strategies aimed at mitigating chemotherapy-induced neurotoxicity (such as using Nrf-2 activators) while retaining the anti-cancer efficacy of the regimen.

Abbreviations

ANOVA, Analysis employed in this study for the biochemical measurements was conducted using one-way analysis of variance; ARE, Antioxidant response elements; BBB, Blood-brain barrier; CIPN, Chemotherapy-induced peripheral neuropathy; CNS, Central nervous system; GFAP, Glial fibrillary acidic protein; H&E, Hematoxylin and eosin; HPLC, High-performance liquid chromatography; LOD, Limits of detection; NCAM, Neural adhesion molecule; ROS, Reactive oxygen species; RSD, Relative standard deviation; SDS, Sodium dodecyl sulfate; TAC, Total Antioxidant Capacities; TBA, The reaction between thiobarbituric acid.

Data Sharing Statement

Data generated and/or analyzed during this study are available from the corresponding authors upon reasonable request.

Acknowledgments

The authors extend their appreciation to Prince Sattam bin Abdulaziz University for funding this research work through the project number PSAU/2024/01/825303.

Funding

This research was funded by Prince Sattam bin Abdulaziz University through the project number PSAU/2024/01/825303.

Disclosure

The authors report no conflicts of interest in this work.

References

1. Sung H, Ferlay J, Siegel RL, et al. Global cancer statistics 2020: GLOBOCAN estimates of incidence and mortality worldwide for 36 cancers in 185 countries. *Canc J Clin*. 2021;71(3):209–249. doi:10.3322/caac.21660
2. Lustberg MB, Kuderer NM, Desai A, et al. Mitigating long-term and delayed adverse events associated with cancer treatment: implications for survivorship. *Nat Rev Clin Oncol*. 2023;20(8):527–542. doi:10.1038/s41571-023-00776-9
3. Khasraw M, Posner JB. Neurological complications of systemic cancer. *The Lancet Neurology*. 2010;9(12):1214–1227. doi:10.1016/S1474-4422(10)70220-9
4. Nguyen LD, Ehrlich BE. Cellular mechanisms and treatments for chemobrain: insight from aging and neurodegenerative diseases. *EMBO Mol Med*. 2020;12(6):e12075. doi:10.15252/emmm.202012075
5. El-Agamy SE, Abdel-Aziz AK, Esmat A, et al. Chemotherapy and cognition: comprehensive review on doxorubicin-induced chemobrain. *Cancer Chemother Pharmacol*. 2019;84(1):1–14. doi:10.1007/s00280-019-03827-0
6. Kogan LG, Davis SL, Brooks GA. Treatment delays during FOLFOX chemotherapy in patients with colorectal cancer: a multicenter retrospective analysis. *J Gastrointestinal Oncol*. 2019;10(5):841–846. doi:10.21037/jgo.2019.07.03
7. Hu S, Liu K, Luo H, et al. Caffeine programs hepatic SIRT1-related cholesterol synthesis and hypercholesterolemia via A2AR/cAMP/PKA pathway in adult male offspring rats. *Toxicology*. 2019;418:11–21. doi:10.1016/j.tox.2019.02.015
8. Blondy S, David V, Verdier M, et al. 5-fluorouracil resistance mechanisms in colorectal cancer: from classical pathways to promising processes. *Cancer Sci*. 2020;111:3142–3154
9. Długosz-Pokorska A, Perlikowska R, Janecki T,et al. New uracil analog with exocyclic methylidene group can reverse resistance to taxol in MCF-7 cancer cells. *Biologics*. 2023:69.
10. Tarbit E, Singh I, Peart JN, et al. Biomarkers for the identification of cardiac fibroblast and myofibroblast cells. *Heart Failure Reviews*. 2019;24(1):1–15. doi:10.1007/s10741-018-9720-1
11. McIlwain DR, Berger T, Mak TW. Caspase functions in cell death and disease. *Cold Spring Harbor Perspectives Biol*. 2013;5(4):1–28. doi:10.1101/cshperspect.a008656
12. Wang YW, Dong H-Z, Tan Y-X, et al. HIF-1α-regulated lncRNA-TUG1 promotes mitochondrial dysfunction and pyroptosis by directly binding to FUS in myocardial infarction. *Cell Death Discov*. 2022;8(1):178. doi:10.1038/s41420-022-00969-8
13. Olufunmilayo EO, Gerke-Duncan MB, Holsinger RMD. Oxidative stress and antioxidants in neurodegenerative disorders. *Antioxidants*. 2023;12(2):517. doi:10.3390/antiox12020517
14. Aboubakr EM, Ibrahim AR, Ali FE,et al. Fasudil ameliorates methotrexate-induced hepatotoxicity by modulation of redox-sensitive signals. *Pharmaceuticals*. 2022;15(11):1436.
15. Itoh K, Mimura J, Yamamoto M. Discovery of the negative regulator of Nrf2, keap1: a historical overview. *Antioxidants Amp*. 2010;13(11):1665–1678. doi:10.1089/ars.2010.3222
16. Abdulaal WH, Asfour HZ, Helmi N, et al. Capsaicin ameliorate pulmonary fibrosis via antioxidant Nrf-2/ PPAR- γ pathway activation and inflammatory TGF-β1/ NF-κB/COX II pathway inhibition. *Front Pharmacol*. 2024;15:1333715.
17. Cook KL, Clarke PAG, Parmar J, et al. Knockdown of estrogen receptor-α induces autophagy and inhibits antiestrogen-mediated unfolded protein response activation, promoting ROS-induced breast cancer cell death. *THE FASEB Journal*. 2014;28(9):3891–3905. doi:10.1096/fj.13-247353
18. Jiang T, Harder B, Rojo de la Vega M, et al. p62 links autophagy and Nrf2 signaling. *Free Radical Biol Med*. 2015;88:199–204. doi:10.1016/j.freeradbiomed.2015.06.014
19. Bhattacharyya A, Chattopadhyay R, Mitra S, et al. Oxidative stress: an essential factor in the pathogenesis of gastrointestinal mucosal diseases. *Physiol Rev*. 2014;94(2):329. doi:10.1152/physrev.00040.2012
20. Melnik EV, Petukhov AE, Kozin SV, et al. Validated HPLC-MS/MS method for quantification of ethylmethylhydroxypyridine succinate in rat brain and its application to a pharmacokinetic study. *J Chromatogr B Analyt Technol Biomed Life Sci*. 2018;1096:180–186. doi:10.1016/j.jchromb.2018.08.029
21. Beraza E, Serrano-Civantos M, Izco M, et al. High-performance liquid chromatography–fluorescence detection method for ochratoxin a quantification in small mice sample volumes: versatile application across diverse matrices relevant for neurodegeneration research. *Toxins*. 2024;16(5):213. doi:10.3390/toxins16050213
22. Wróblewski K, Petruczynik A, Radzik I, et al. Determination of selected antiepileptic drugs in mouse brain homogenates by HPLC—DAD. *Acta Chromatographica*. 2017;29(2):219–234. doi:10.1556/1326.2017.29.2.6

23. Viljoen F, Du Preez JL, Wessels JC, et al. HPLC electrochemical detection and quantification of monoamines and their metabolites in rat brain tissue samples. *Die Pharmazie-An Int J Pharmac Sci*. 2018;73(10):563–569.
24. Guiard BP, Gotti G. The high-precision liquid chromatography with electrochemical detection (HPLC-ECD) for monoamines neurotransmitters and their metabolites: a review. *Molecules*. 2024;29(2):496. doi:10.3390/molecules29020496
25. El Zahar NM, Sutton JM, Bartlett MG. Assessment of brain-to-blood drug distribution using liquid chromatography. *Biomed Chromatography*. 2021;35(7):e5123. doi:10.1002/bmc.5123
26. Maher HM, Mohamed SM, Hassan EM, et al. Sustainability-based comparative stability of oxaliplatin plus leucovorin and 5-fluorouracil in infusion bags with application to plasma and colonic media samples. *Scientific Rep*. 2025;15(1):17982. doi:10.1038/s41598-025-02079-8
27. Shahi S, Ang CS, Mathivanan S. A High-Resolution mass spectrometry-based quantitative metabolomic workflow highlights defects in 5-fluorouracil metabolism in cancer cells with acquired chemoresistance. *Biology*. 2020;9(5):96. doi:10.3390/biology9050096
28. Zimmermann M. Ethical guidelines for investigations of experimental pain in conscious animals. *Pain*. 1983;16(2):109–110. doi:10.1016/0304-3959(83)90201-4
29. Robinson SM, Mann J, Vasilaki A, et al. Pathogenesis of FOLFOX induced sinusoidal obstruction syndrome in a murine chemotherapy model. *J Hepatol*. 2013;59(2):318–326. doi:10.1016/j.jhep.2013.04.014
30. Di cesare mannelli L, Maresca M, Micheli L, et al. A rat model of FOLFOX-induced neuropathy: effects of oral dimiracetam in comparison with duloxetine and pregabalin. *Cancer Chemother Pharmacol*. 2017;80(6):1091–1103. doi:10.1007/s00280-017-3449-8
31. Ruvinov I, et al. Lemongrass extract possesses potent anticancer activity against human colon cancers, inhibits tumorigenesis, enhances efficacy of FOLFOX, and reduces its adverse effects. *Integr Cancer Ther*. 2019; 18:1534735419889150
32. Prakoso YA, Sigit M, Aliviameita A. Standardization of the simple methodology for experimentally induced ischemic stroke in rat models. *World's Veterinary J*. 2023;13(4):510–519. doi:10.54203/scil.2023.wvj54
33. Khalil HM, Salama HH, Al-Mokaddem AK, et al. Edible dairy formula fortified with coconut oil for neuroprotection against aluminium chloride-induced Alzheimer's disease in rats. *J Functional Foods*. 2020;75:104296. doi:10.1016/j.jff.2020.104296
34. Ericson E, Samuelsson J, Ahlenius S. Photocell measurements of rat motor activity. A contribution to sensitivity and variation in behavioral observations. *J Pharmacol Methods*. 1991;25(2):111–122. doi:10.1016/0160-5402(91)90002-M
35. Mohamed DM, Shaqura M, Li X, et al. Aldosterone synthase in peripheral sensory neurons contributes to mechanical hypersensitivity during local inflammation in rats. *Anesthesiology*. 2020;132(4):867–880. doi:10.1097/ALN.0000000000003127
36. Necker R, Hellon RF. Noxious thermal input from the rat tail: modulation by descending inhibitory influences. *Pain*. 1978;4(3):231–242. doi:10.1016/0304-3959(77)90135-X
37. Mangaiarkkarasi A, Rameshkannan S, Ali RM. Effect of gabapentin and pregabalin in rat model of taxol induced neuropathic pain. *J Clin Diagn Res*. 2015;9(5):p.FF11–4.
38. Peskin AV, Winterbourn CC. A microtiter plate assay for superoxide dismutase using a water-soluble tetrazolium salt (WST-1). *Clin Chim Acta*. 2000;293(1–2):157–166. doi:10.1016/S0009-8981(99)00246-6
39. Draper HH, Squires EJ, Mahmoodi H, et al. A comparative evaluation of thiobarbituric acid methods for the determination of malondialdehyde in biological materials. *Free Radic Biol Med*. 1993;15(4):353–363. doi:10.1016/0891-5849(93)90035-S
40. Bryan NS, Grisham MB. Methods to detect nitric oxide and its metabolites in biological samples. *Free Radic Biol Med*. 2007;43(5):645–657. doi:10.1016/j.freeradbiomed.2007.04.026
41. Razygraev AV, Taborskaya KI, Petrosyan MA, et al. Thiol peroxidase activities in rat blood plasma determined with hydrogen peroxide and 5,5`-dithio-bis(2-nitrobenzoic acid). *Biomed Khim*. 2016;62(4):431–438. doi:10.18097/PBMC20166204431
42. Andziak B, O'Connor TP, Buffenstein R. Antioxidants do not explain the disparate longevity between mice and the longest-living rodent, the naked mole-rat. *Mech Ageing Dev*. 2005;126(11):1206–1212. doi:10.1016/j.mad.2005.06.009
43. Rahman I, Kode A, Biswas SK. Assay for quantitative determination of glutathione and glutathione disulfide levels using enzymatic recycling method. *Nat Protoc*. 2006;1(6):3159–3165. doi:10.1038/nprot.2006.378
44. Borman P, Elder D. Q2(R1) validation of analytical procedures. *ICH Quality Guidelines*. 2017;127–166.
45. Siegel RL, Giaquinto AN. Cancer Statistics. *Cancer J Clin*. 2024;74(1).
46. Sidaway PJNRCO. FOLFOX–HAIC active in large HCC. *Nat Rev Clin Oncol*. 2022;19(1):5.
47. Park D, Baek S-J, Kwak J-M, et al. Analysis of reduced-dose administration of oxaliplatin as adjuvant FOLFOX chemotherapy for colorectal cancer. *Ann Surg Treat Res*. 2018;94(4):196–202. doi:10.4174/astr.2018.94.4.196
48. Maihöfner C, Diel I, Tesch H, et al. Chemotherapy-induced peripheral neuropathy (CIPN): current therapies and topical treatment option with high-concentration capsaicin. *Supportive Care Cancer*. 2021;29(8):4223. doi:10.1007/s00520-021-06042-x
49. Areti A, Yerra VG, Naidu V, et al. Oxidative stress and nerve damage: role in chemotherapy induced peripheral neuropathy. *Redox Biology*. 2014;2:289. doi:10.1016/j.redox.2014.01.006
50. Was H, Borkowska A, Bagues A, et al. Mechanisms of chemotherapy-induced neurotoxicity. *Front Pharmacol*. 2022;13.
51. Basu P, Averitt DL, Maier C, et al. The effects of Nuclear Factor Erythroid 2 (NFE2)-Related Factor 2 (Nrf2) activation in preclinical models of peripheral neuropathic pain. *Antioxidants*. 2022;11(2):430. doi:10.3390/antiox11020430
52. Verri WA, Vicentini FT, Baracat MM, et al. Flavonoids as anti-inflammatory and analgesic drugs: mechanisms of action and perspectives in the development of pharmaceutical forms. *Studies Nat Produc Chem*. 2012;36:297–330.
53. Ngo V, Duennwald MLJA. Nrf2 and oxidative stress: a general overview of mechanisms and implications in human disease. *Antioxidants*. 2022;11(12):2345. doi:10.3390/antiox11122345
54. Petrikonis K, Bernatoniene J, Kopustinskiene DM, et al. The antinociceptive role of Nrf2 in neuropathic pain: from mechanisms to clinical perspectives. *Pharmaceutics*. 2024;16(8):1068. doi:10.3390/pharmaceutics16081068
55. Ogura T, Tong KI, Mio K, et al. Keap1 is a forked-stem dimer structure with two large spheres enclosing the intervening, double glycine repeat, and C-terminal domains. *Proc Nat Acad Sci*. 2010. 107: p. 2842–2847.
56. Vasconcelos AR, Wang Z, Peng Y, et al. Nrf2/ARE pathway modulation by dietary energy regulation in neurological disorders. *Front Pharmacol*. 2019;10:10. doi:10.3389/fphar.2019.00010
57. Nguyen T, Nioi P, Pickett CB.et al. The Nrf2-antioxidant response element signaling pathway and its activation by oxidative stress. *J Biol Chem*. 2009;284(20):13291–13295

58. Ruiz S, Pergola PE, Zager RA, et al. Targeting the transcription factor Nrf2 to ameliorate oxidative stress and inflammation in chronic kidney disease. *Kidney International*. 2013;83(6):1029–1041. doi:10.1038/ki.2012.439
59. Loboda A, Damulewicz M, Pyza E, et al. Role of Nrf2/HO-1 system in development, oxidative stress response and diseases: an evolutionarily conserved mechanism. *Cell Mol Life Sci*. 2016;73(17):3221–3247. doi:10.1007/s00018-016-2223-0
60. Fumagalli G, Monza L, Cavaletti G, et al. Neuroinflammatory process involved in different preclinical models of chemotherapy-induced peripheral neuropathy. *Front Immunol*. 2021;11:p.626687. doi:10.3389/fimmu.2020.626687
61. Zitvogel L, Apetoh L, Ghiringhelli F,et al. Immunological aspects of cancer chemotherapy. *Nat Rev Immunol*. 2008;8(1):59–73.
62. Makker PG, Duffy SS, Lees JG, et al. Characterisation of immune and neuroinflammatory changes associated with chemotherapy-induced peripheral neuropathy. *PLoS One*. 2017;12(1):e0170814.
63. Norden DM, Trojanowski PJ, Villanueva E, et al. Sequential activation of microglia and astrocyte cytokine expression precedes increased iba-1 or GFAP immunoreactivity following systemic immune challenge. *Glia*. 2016;64(2):300–316. doi:10.1002/glia.22930
64. Eng LF, Ghirnikar RS, Lee YL. Glial fibrillary acidic protein: GFAP-thirty-one years (1969-2000). *Neurochemical Res*. 2000;25(9–10):1439–1451. doi:10.1023/A:1007677003387
65. Barthel PC, Staabs F, Li LY, et al. Immunoreactivity to astrocytes in different forms of dementia: high prevalence of autoantibodies to GFAP. *Brain Behavior Immunity Health*. 2023;29.
66. Shen X-N, Huang S-Y, Cui M, et al. Plasma glial fibrillary acidic protein in the alzheimer disease continuum: relationship to other biomarkers, differential diagnosis, and prediction of clinical progression. *Clinical Chemistry*. 2023;69(4):411–421. doi:10.1093/clinchem/hvad018
67. Khan Z, Gupta GD, Mehan SJJOCM. Cellular and molecular evidence of multiple sclerosis diagnosis and treatment challenges. *J Clin Med*. 2023;12(13):4274. doi:10.3390/jcm12134274
68. Sytnyk V, Leshchyns'ka I, Schachner M. Neural cell adhesion molecules of the immunoglobulin superfamily regulate synapse formation, maintenance, and function. trends in neurosciences. *Trend Neurosci*. 2017;40(5):295–308. doi:10.1016/j.tins.2017.03.003
69. Sowparani S, Mahalakshmi P, Sweety JP, et al. Ubiquitous neural cell adhesion molecule (NCAM): potential mechanism and valorisation in cancer pathophysiology, drug targeting and molecular transductions. *Molecular Neurobiol*. 2022;59(9):5902–5924. doi:10.1007/s12035-022-02954-9
70. Kikuchi T, Shimizu T. Polysialylated NCAM distinguishes differentiated myoblasts from proliferating myoblasts prior to fusion. 2025;647904.
71. Taylor L, Wankell M, Saxena P, et al. Cell adhesion an important determinant of myogenesis and satellite cell activity. *Biochimica Et Biophysica Acta*. 2022;1869(2):119170. doi:10.1016/j.bbamcr.2021.119170
72. Parcerisas A, Ortega-Gascó A, Pujadas L, et al. The hidden side of NCAM family: NCAM2, a key cytoskeleton organization molecule regulating multiple neural functions. *Int J Mol Sci*. 2021;22(18):10021. doi:10.3390/ijms221810021
73. Croce CM, Vaux D, Strasser A, et al. The BCL-2 protein family: from discovery to drug development. *Cell Death Differ*. 2025;1–13.
74. Marie Hardwick J, Soane L. Multiple functions of BCL-2 family proteins. *Cold Spring Harbor Perspect Biol*. 2013;5.
75. Czabotar PE, Garcia-Saez AJ. Mechanisms of BCL-2 family proteins in mitochondrial apoptosis. *Nat Rev Mol Cell Biol*. 2023;24(10):732–748.
76. Qian S, Wei Z, Yang W, et al. The role of BCL-2 family proteins in regulating apoptosis and cancer therapy. *Front Oncol*. 2022;12.
77. Arvanitis M, Li DD, Lee K, et al. Apoptosis in c.elegans: lessons for cancer and immunity. *Front Cell Infect Microbiol*. 2013;4:65621.
78. Tehranian R, Rose ME, Vagni V, et al. Transgenic mice that overexpress the anti-apoptotic bcl-2 protein have improved histological outcome but unchanged behavioral outcome after traumatic brain injury. *Brain Research*. 2006;1101(1)::126–135
79. Sahoo G, Samal D, Khandayataray P, et al. A review on caspases: key regulators of biological activities and apoptosis. *Mol Neurobiol*. 2023;60 (10):5805–5837. doi:10.1007/s12035-023-03433-5
80. Wang Y, Gu J, Hu L, et al. miR-130a alleviates neuronal apoptosis and changes in expression of Bcl-2/Bax and caspase-3 in cerebral infarction rats through PTEN/PI3K/Akt signaling pathway. *Exp Ther Med*. 2020;19(3):2119–2126. doi:10.3892/etm.2020.8415
81. Teixeira C, Florencio-Silva R, Sasso GRS, et al. Soy isoflavones protect against oxidative stress and diminish apoptosis in ovary of middle-aged female rats. *Gynecological Endocrinol*. 2019;35(7):586–590. doi:10.1080/09513590.2018.1559287
82. Stoian M, Dumitrache AM, Cîrciu F, et al. Apoptosis in acute kidney injury. *Intern Med*. 2020;17(1):45–53.
83. Zhou Z, Arroum T, Luo X, et al. Diverse functions of cytochrome c in cell death and disease. *Cell Death Differentiation*. 2024;31(4):387–404. doi:10.1038/s41418-024-01284-8
84. Singh S, Singh TGJIR. Emerging perspectives on mitochondrial dysfunctioning and inflammation in epileptogenesis. *Inflamm Res*. 2021;70 (10):1027–1042. doi:10.1007/s00011-021-01511-9